Journal of Magnetic Resonance 203 (2010) 113–128

Contents lists available at ScienceDirect

Journal of Magnetic Resonance

journal homepage: www.elsevier.com/locate/jmr

Homonuclear dipolar recoupling under ultra-fast magic-angle spinning: Probing $^{19}F-^{19}F$ proximities by solid-state NMR

Qiang Wang [a,b,c], Bingwen Hu [a], Olivier Lafon [a], Julien Trébosc [a], Feng Deng [b,*], Jean-Paul Amoureux [a,*]

[a] UCCS, CNRS-8181, Lille-University, 59652, Villeneuve d'Ascq, France
[b] State Key Laboratory of Magnetic Resonance and Atomic and Molecular Physics, Wuhan Center for Magnetic Resonance, WIPM, Chinese Academy of Sciences, Wuhan 430071, China
[c] Graduate School of the Chinese Academy of Sciences, Beijing, China

ARTICLE INFO

Article history:
Received 5 November 2009
Revised 9 December 2009
Available online 14 December 2009

Keywords:
Solid-state NMR
Double quanta
Ultra-fast MAS
^{1}H and ^{19}F
High field magnet

ABSTRACT

We describe dipolar recoupling methods that accomplish, at high magic-angle spinning (MAS) frequencies, the excitation of double-quantum (DQ) coherences between spin-1/2 nuclei. We employ rotor-synchronized symmetry-based pulse sequences which are either γ-encoded or non-γ-encoded. The sensitivity and the robustness to both chemical-shift anisotropy and offset are examined. We also compare different techniques to avoid signal folding in the indirect dimension of two-dimensional double-quantum ↔ single-quantum (DQ–SQ) spectra. This comprehensive analysis results in the identification of satisfactory conditions for dipolar $^{19}F-^{19}F$ recoupling at high magnetic fields and high MAS frequencies. The utility of these recoupling methods is demonstrated with high-resolution DQ–SQ NMR spectra, which allow probing $^{19}F-^{19}F$ proximities in powered fluoroaluminates.

1. Introduction

One of the frontiers in solid-state NMR is the development of recoupling and decoupling methods, compatible with high magic-angle spinning (MAS) frequencies of 30 kHz and greater. Recently, the reduction of rotor diameter has led to a considerable increase of sample spinning frequency. For instance, ultra-fast MAS frequencies, larger than 60 kHz, can now be reached easily by employing commercial rotors with outer diameters (o.d.) of 1.2–1.3 mm.

One of the key advantages of high MAS frequencies is the better average of large dipolar interactions. This leads to a gain in resolution, sensitivity per spin and transverse relaxation time, especially in the case of ^{1}H and ^{19}F nuclei, which are submitted to large dipolar interactions [1–3]. Furthermore, ultra-fast MAS (i) minimizes spinning sidebands arising from chemical-shift anisotropy (CSA), (ii) allows low-power radio frequency (rf) decoupling schemes, and (iii) increases the spectral width (SW_1) in the indirect dimension of rotor-synchronized experiments. Last, small rotor o.d. leads to the ability of generating very high rf magnetic fields. These specifications are advantageous for isotopes, such as ^{19}F, which exhibit large CSA and extended ranges of isotropic chemical shifts ($\Delta\nu_{iso}$).

In the presence of MAS, dipolar recoupling sequences are required to reintroduce the dipole–dipole couplings, which are averaged out by MAS. These methods allow probing the inter-nuclear proximities [4–22]. In particular, they are essential when efficient coherence transfers through the *J*-couplings are precluded, as in the case of ^{1}H, ^{19}F and quadrupolar nuclei [19,21,22]. In the following, we will focus on double-quantum (DQ) homonuclear dipolar recoupling sequences, which allow the excitation of DQ coherences (DQC) between isotopes with the same atomic number. These recoupling methods can be incorporated into two-dimensional (2D) NMR experiments, which correlate DQC with single-quantum coherences (SQC) within each homonuclear spin pair. Compared to SQ–SQ homonuclear correlation (HOMCOR) experiments, DQ–SQ HOMCOR spectroscopy benefits from the possibility to probe proximities between sites with identical or close resonance frequencies [23].

However, at high spinning frequencies, the use of well-established homonuclear dipolar recoupling methods, such as symmetry-based pulse sequences [11–13,15–18], is limited by the requirement of high-power rf field, which is proportional to the MAS frequency, ν_R. The Back-to-Back (BABA) scheme, which emerged in the mid-1990s [8,9], is presently one of the most popular DQ homonuclear dipolar recoupling sequences under fast and ultra-fast MAS ($\nu_R > 30$ kHz). This technique has been used mainly to observe $^{1}H-^{1}H$ and $^{19}F-^{19}F$ correlations [8,9,24–26]. Nevertheless, it suffers from two major drawbacks. First, it is not robust to CSA and to large differences in resonance frequencies ($\Delta\nu_{iso}$). Second, it does not display the property called "γ-encoding" since the recoupled dipolar Hamiltonian is amplitude-modulated by the Euler angle, γ_{MR}, which is one of the three angles defining the orientation of the molecule in the rotor-fixed frame [10,15,17]. The presence of "γ-encoding" leads (i) to a ≈20% increase of theoretical maximum efficiency of DQ-filtered (DQF) experiments

* Corresponding authors.
E-mail addresses: dengf@wipm.ac.cn (F. Deng), jean-paul.amoureux@univ-lille1.fr (J.-P. Amoureux).

1090-7807/$ - see front matter © 2009 Elsevier Inc. All rights reserved.
doi:10.1016/j.jmr.2009.12.009

in powder samples, and (ii) to larger oscillations of this DQF signal as function of the recoupling periods, which allows determining inter-nuclei distances with greater accuracy [10,15,17]. Furthermore, for non-γ-encoded recoupling sequences, the interval between the excitation and reconversion parts has to be an integer multiple of the rotor period. Therefore, in usual DQ–SQ NMR experiments, the spectral width in the indirect dimension (SW_1) is restricted to submultiples of ν_R.

Recently we have proposed an alternative to BABA recoupling by introducing the Sandwiched PI pulse (SPIP) scheme [19,22] The SPIP method is a super-cycled version of the $R2_2^1$ symmetry-based pulse sequence. We have demonstrated that this sequence is compatible with ultra-fast MAS. Furthermore, it displays higher robustness to CSA and offset than BABA. This allows the observation of $^{19}F-^{19}F$ proximities, although these nuclei are submitted to large magnetic shielding. Yet the SPIP recoupling is not γ-encoded. In the meantime, it was shown that $R12_2^5$ and $R14_4^5$ symmetry-based sequences accomplish $^1H-^1H$ dipolar recoupling at $\nu_R = 67$ kHz [18]. These γ-encoded methods provide higher DQF efficiency than BABA but their robustness to offset and CSA has not been investigated so far.

The present article provides a comprehensive comparison of γ-encoded and non-γ-encoded DQ homonuclear dipolar recoupling methods at high MAS frequencies. In particular, we analyze their DQF efficiency as well as their robustness to offset and CSA. Robust γ-encoded recoupling sequences compatible with ultra-fast MAS are introduced by combining symmetry principles and appropriate composite pulses. These novel recoupling methods are employed to obtain high-resolution $^{19}F-^{19}F$ DQ–SQ spectra of inorganic fluoroaluminates. Different techniques to avoid signal folding in the DQ indirect dimension are also examined.

2. Pulse sequences

2.1. Symmetry-based DQ dipolar recoupling sequences

A DQ dipolar recoupling sequence compatible with high MAS frequencies should ideally possess the following properties: (i) the rf-power requirements are below the usual probe specifications, (ii) the sequence provides the highest achievable DQF efficiency, (iii) it is robust to offset, CSA and rf imperfections and (iv) the magnitude of the recoupled dipolar interaction is much lower than the inverse of the recoupling cycle time, i.e. the maximal sampling frequency of the DQC build-up curve. In particular the criterion (iii) is critical when the recoupling sequence is applied to nuclei exhibiting large CSA as well as a large spread of resonance frequencies. This will be illustrated in the present article by dipolar $^{19}F-^{19}F$ recoupling in inorganic fluoroaluminates. In that case, the CSA is typically in the order of 100 ppm, while the isotropic chemical shifts (δ_{iso}) can span over more than 100 ppm [22]. Therefore, at large static magnetic fields, e.g. $B_0 = 18.8$ T, the magnitude of CSA and offset interactions can reach at least 75 kHz, whereas the largest $^{19}F-^{19}F$ dipolar coupling constants are about $b_{jk}/(2\pi) = -7$ kHz ($d_{jk} = 250$ pm).

The interferences of unwanted interactions can be limited by employing symmetry arguments for the design of the recoupling sequences [11–13,15–18]. These symmetry-based methods comprise both CN_n^ν and RN_n^ν classes. We will only consider, in this article, recoupling sequences deriving from RN_n^ν symmetries, which benefit from more restrictive selection rules than CN_n^ν sequences and hence are usually more robust [12]. The RN_n^ν pulse sequences, depicted in Fig. 1f, are composed of $N/2$ $R_{\pi\nu/N}R'_{-\pi\nu/N}$ inversion cycle pairs, spanning n rotor periods. The prime indicates a change in the sign of all phases internal to the basic inversion element R. The R_0 element rotates the resonant nuclear spins by an odd multiple of π about the x-axis of the rotating frame. It may be a single or a composite π pulse or a suitable amplitude, phase and/or frequency modulation scheme, lasting nT_R/N.

The spin dynamics during RN_n^ν pulse sequences can be described in the framework of average Hamiltonian theory (AHT) [15]. For a homonuclear spin pair, I_j and I_k, the first-order average Hamiltonian of homonuclear dipolar DQ recoupling must contain terms proportional to the DQ operators $I_j^\pm I_k^\pm$. The magnitude of these DQ recoupled dipolar interactions governs the optimal recoupling time. The choice of the RN_n^ν symmetry and of the basic element affects the magnitude of the recoupled dipolar interactions by

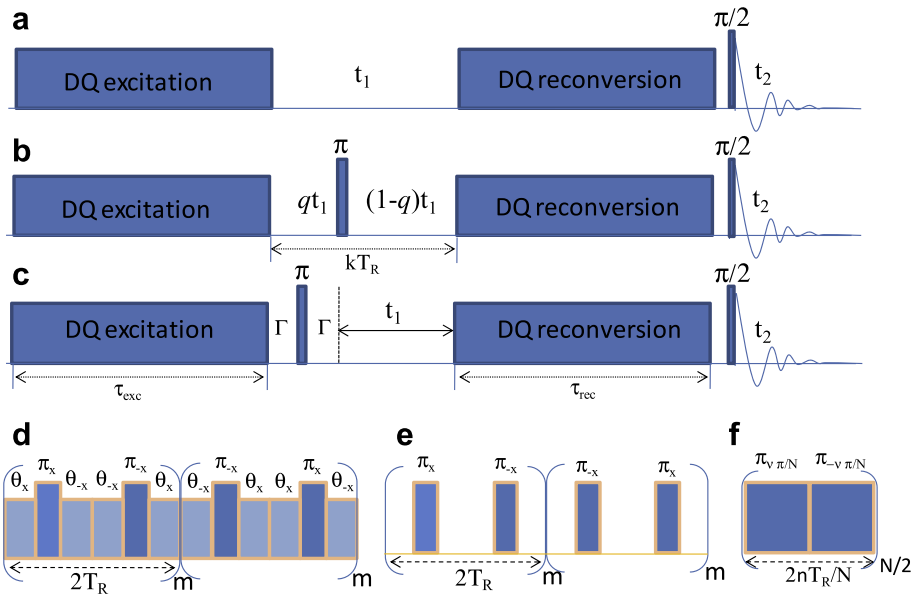

Fig. 1. (a–c) General DQ–SQ pulse schemes. (a) This scheme can be used either for γ-encoded sequences or non-γ-encoded sequences if the evolution time is rotor-synchronized: $t_1 = kT_R$. In the present article, the excitation and reconversion delays are identical, $\tau_{exc} = \tau_{rec} = \tau$. (b and c) Schemes that can be used with non-γ-encoded sequences if the F_1 spectral width is insufficient to avoid foldings. In both cases, the delay between the excitation and reconversion periods must be rotor-synchronized (kT_R), and a π pulse has been added. There are either (b) two evolution periods qt_1 and $(1-q)t_1$, or (c) only one evolution period t_1 and two short delays Γ sandwiching the π pulse and calculated according to Eq. (6). (d–f) Homonuclear recoupling sequences: (d) SPIP, (e) $BR2_2^1$, and (f) RN_n^ν .

modifying the scaling factors $\kappa_{lm\lambda\mu}$ of symmetry-allowed terms [15]. For homonuclear dipolar DQ recoupling, the quantum numbers $\{l, m, \lambda, \mu\}$ are restricted to $\{2, m, 2, \pm 2\}$ with $m = \pm 1$ and ± 2. The strength of the recoupled DQ interaction can be assessed by calculating the root mean square (rms) of the scaling factors:

$$\kappa_{DD2Q}^{rms} = \left(\sum_m \left[|\kappa_{2m22}|^2 + |\kappa_{2m2-2}|^2 \right] \right)^{1/2} \quad (1)$$

where the sum is taken over $m = \pm 1$ and ± 2. Formulae for scaling factors are given in Ref. [27]. They were determined by employing the 'C and R symmetries' Mathematica package which takes into account the possible super-cycle [12,13,27–29]. The optimal recoupling time, leading to maximal DQF efficiency, decreases with increasing κ_{DD2Q}^{rms} scaling factor (see Eq. (5)). Therefore, large κ_{DD2Q}^{rms} values allow reducing the irreversible losses during the recoupling times and hence enhance the DQF efficiency, provided the recoupled dipolar interaction remains lower than the sampling frequency of the DQC build-up curve.

2.2. Non-γ-encoded recoupling sequences

Two non-γ-encoded recoupling methods were employed, SPIP and $BR2_2^1$ [19,20]. Both of these methods, depicted in Fig. 1d and e, respectively, derive from $R2_2^1$ symmetry. The basic $R2_2^1$ scheme spanning two rotor periods, accomplishes both 0Q and 2Q dipolar recoupling [30]. However, it does not eliminate the unwanted CSA and offset terms in the first-order average Hamiltonian. We have shown that the robustness to CSA and offset is increased by applying an overall phase shift of 180° from the middle of the recoupling sequence [19,20]. These block-super-cycled methods spanning $4p$ rotor periods may be written explicitly as follows:

$$\left(R2_2^1\right)^p \left(R2_2^{-1}\right)^p = R2P_{2p}^p R2P_{2p}^{-p} \quad (2)$$

The only difference between SPIP and $BR2_2^1$ schemes lies in the basic inversion element, R. SPIP and $BR2_2^1$ sequences are based on $R = \theta_0 180_0 \theta_{180}$ and $\tau - 180_0 - \tau$, respectively. Here, ξ_φ indicates a rectangular, resonant rf pulse with flip angle ξ and phase φ, and τ is a window delay during which no rf field is applied [15]. In the SPIP sequence, the use of spin-lock periods with flip-angles θ allows decreasing the irreversible losses, when the $T_{1\rho}$ relaxation time is much larger than the T_2' constant time [19]. The performances of SPIP and $BR2_2^1$ depend on the relative durations of the π pulse, τ_π, and the rotor period, T_R, i.e. the pulse fraction $f = \tau_\pi / T_R$. Globally, the use of low f fraction, i.e. strong π pulses, increases the robustness to offset and CSA, but decreases the κ_{DD2Q}^{rms} scaling factor [20]. Therefore, the optimal pulse fraction ($f \approx 0.2$–0.3) results from a compromise between the irreversible losses and the CSA and offset interferences. Typical values of κ_{DD2Q}^{rms} parameters for SPIP and $BR2_2^1$ schemes are reported in Table 1.

2.3. γ-Encoded recoupling sequences and composite π pulses

For ideal γ-encoded DQ recoupling sequences, if the homonuclear J-coupling is disregarded, the first-order average Hamiltonian of an isolated spin pair I_j and I_k must contain only pure DQ terms

$$\overline{H}^{(1)} = \overline{\omega}_{2m22}^{jk} I_j^+ I_k^+ + \overline{\omega}_{2m22}^{jk*} I_j^- I_k^- \quad (3)$$

where $m = \pm 1$ or ± 2, depending on the pulse sequence symmetry. For γ-encoded recoupling, the complex amplitudes, $\overline{\omega}_{2m22}^{jk}$ and $\overline{\omega}_{2m22}^{jk*}$, depend on the Euler angle, γ_{MR}, through their arguments (called phases) but not through their amplitudes.

A large number of RN_n^ν sequences achieve γ-encoded DQ recoupling. A selection of RN_n^ν symmetries with $n \leqslant 10$ and $N \leqslant 30$ was given in Ref. [31]. However, not all the types of symmetry can be employed at high MAS frequencies owing to the limited probe performances in terms of rf field. For instance, an o.d. 2.5 and 1.2–1.3 mm MAS probe can reasonably deliver, during the recoupling interval, ^{19}F nutation frequencies, ν_1, up to 160 and 230 kHz, respectively. Therefore, when the rotor with o.d. 2.5 mm (resp. 1.2–1.3 mm) spins at $\nu_R \approx 32$ (resp. 65 kHz), only recoupling schemes requiring ν_1/ν_R ratios lower than 5 (resp. 3.5) can be employed. The ν_1 parameter depends upon the RN_n^ν symmetry and the basic element, R. For instance, for RN_n^ν sequences based on the element $R = 180_0$, the required rf nutation frequency is equal to $\nu_1(180) = N\nu_R/(2n)$. Recently, it was demonstrated that $R12_2^5$ and $R14_4^5$ pulse sequences using $R = 180_0$ achieve efficient $^1H-^1H$ DQ recoupling at $\nu_R = 67$ kHz [18]. However, we show below that the DQF efficiencies of these sequences are greatly affected by offsets larger than 5 kHz. Therefore, $R12_2^5$ and $R14_4^5$ schemes may not be suitable for isotopes, such as ^{19}F, ^{13}C or ^{31}P, which exhibit a large range of shifts.

The robustness to offset of γ-encoded recoupling sequences can be improved by the use of broadband composite pulse as basic element [15,32]. The gain in robustness is achieved at the cost of a larger rf-power requirement. The increase in rf nutation frequency between $R = 180_0$ and a composite pulse is

$$\frac{\nu_1(R)}{\nu_1(180)} = \frac{\sum \xi_j}{180} \quad (4)$$

where ξ_j is the flip angle of the jth pulse of the composite pulse and the sum is over all the pulses constituting the R element. The seven tested composite R_p ($p = 1$–7) elements and their $\nu_1(R)/\nu_1(180)$ ratios are listed in Table 2. These composite elements cannot be incorporated into $R12_2^5$ and $R14_4^5$ schemes at $\nu_R = 65$ kHz owing to the limited rf field delivered by the probe. At such high MAS frequencies, the only solution consists in combining these composite pulses with RN_n^ν symmetries displaying lower $\nu_1(180)/\nu_R$ rf requirements, i.e. lower $N/(2n)$ ratios. In the present article, we concentrate on the use of $R14_8^3$, $R18_8^5$ and $R18_{10}^4$ symmetries, which correspond to $\nu_1(180)/\nu_R$ ratios of 0.875, 1.125 and 0.9, respectively. Given the rf-power limitation, at $\nu_R = 65$ kHz composite pulses R_1 to R_6 can be combined with these three symmetries, whereas R_7 element is only compatible with $R14_8^3$ and $R18_{10}^4$.

In order to identify good γ-encoded recoupling sequences, we performed analytical AH calculations up to the second-order. For

Table 1
Properties of the homonuclear dipolar DQ recoupling sequences employed in this article.

Scheme	ν_1 (kHz)[a]	κ_{DD2Q}^{rms}	τ^{opt} (μs)[b]
SPIP	73[c]	0.047	
	103[d]	0.028	
$BR2_2^1$	37.5[c]	0.080	
	60[d]	0.114	
$R12_2^5$[e]	$3\nu_R$	0.246	126
$R14_4^5$[e]	$1.75\nu_R$	0.237	131
$R14_4^5 c$[f]	$4.1\nu_R$	0.173	180
$R10_4^2 c$[f]	$2.9\nu_R$	0.158	197
$R14_8^3 c$[f]	$2.0\nu_R$	0.127	244
$R18_8^5 c$[f]	$2.6\nu_R$	0.150	207
$R18_{10}^4 c$[f]	$2.1\nu_R$	0.126	246

[a] The ν_1 nutation frequency is defined as $\nu_1^2 = (\tau_E)^{-1} \int_0^{\tau_E} \nu_1^2(t) dt$, where $\tau_E = n T_R/N$ is the duration of a basic element.
[b] The τ_{opt} values are calculated according to Eq. (5) using $b_{jk}/(2\pi) = -9135$ Hz.
[c] $\nu_R = 33$ kHz. For SPIP and $BR2_2^1$, the nutation frequency of π pulses is $\nu_{1\pi} = 85$ kHz, and for SPIP, that of spin-lock is $\nu_{1SL} = 70$ kHz.
[d] $\nu_R = 66$ kHz. For SPIP and $BR2_2^1$: $\nu_{1\pi} = 111$ kHz, and for SPIP: $\nu_{1SL} = 100$ kHz. These parameters are those employed for the numerical simulations of Fig. 2a and b ($\nu_R = 33$ kHz) or Fig. 2c and d ($\nu_R = 66$ kHz).
[e] These sequences use a 180_0 pulse as basic element.
[f] These sequences use a $R_4 = 60_0 300_{180} 60_0$ pulse as basic element.

Table 2
Selection of composite pulses employed in this article.

Notation	Composite pulse	$\nu_1(R)/\nu_1(180)$[a]
R1	90_0270_{180}	2
R2	$90_{90}180_090_{90}$	2
R3	$180_{120}180_{240}180_{120}$	3
R4	$60_0300_{180}60_0$	2.3
R5	$90_0240_{90}90_0$	2.3
R6	$90_{45}90_{135}90_{45}$	1.5
R7	$90_0225_{180}315_0$	3.5

[a] The ratio is calculated according to Eq. (4).

γ-encoded DQ recoupling sequences, the first-order AH is given by Eq. (3), and Eq. (1) becomes $\kappa^{rms}_{DD2Q} = \sqrt{2}|\kappa_{2m22}|$, where $m = 1$ or 2. The calculation of first-order κ^{rms}_{DD2Q} scaling factors allows assessing the optimum recoupling time. If the irreversible losses, the homonuclear *J*-coupling and the interferences arising from offset and CSA are disregarded, the maximal DQF efficiency for an isolated spin pair is reached for an excitation and reconversion intervals equal to [17]:

$$\tau^{opt} = \tau^{opt}_{exc} = \tau^{opt}_{rec} = \frac{1.26}{|\kappa_{2m22}|b_{jk}} = \frac{1.26\sqrt{2}}{\kappa^{rms}_{DD2Q}b_{jk}} \quad (5)$$

where b_{jk} is the dipolar coupling constant in rad s^{-1}. Furthermore, in the frame of AHT, the interferences of offset (resp. CSA) for ^{19}F nuclei mainly result from $\delta_{iso} \times \delta_{iso}$ (resp. CSA × CSA) cross-terms in the second-order AH. Therefore, we also determined the rms scaling factors of $\delta_{iso} \times \delta_{iso}$ and CSA × CSA terms [33]. A comparison of first- and second-order scaling factors for various γ-encoded DQ recoupling is given in the Supplementary Information (SI, Fig. S1). This AHT approach predicts that R_1, R_4 and R_7 composite pulses provide the highest robustness to offset and CSA, especially when compared with that provided by the R = 180 element.

RN^{ν}_{n} symmetries, such as $R10^2_4$, which achieve a simultaneous γ-encoded SQ *and* DQ recoupling, were also investigated. Compared to ideal γ-encoded DQ-only recoupling sequences, they display similar robustness to offset and CSA but slightly smaller on-resonance DQF efficiency. The results obtained for $R10^2_4$ are also presented in the article. This symmetry corresponds to a $\nu_1(180)/\nu_R$ ratio of 1.25.

2.4. 1D DQF and 2D DQ–SQ NMR experiments

The typical scheme of DQ–SQ dipolar homonuclear correlation (*D*-HOMCOR) experiments is described in Fig. 1a. A first *excitation* sequence is applied for an interval τ_{exc} in order to transform the longitudinal magnetization into DQC. A second *reconversion* period of duration τ_{rec}, followed by a $\pi/2$ pulse, transforms the DQC into SQC corresponding to observable transverse magnetization. Signals passing through DQC are selected by a four-step phase cycle of the pulses used for exciting or reconverting the DQC. In this article, we use equal excitation and reconversion intervals: $\tau = \tau_{exc} = \tau_{rec}$. For one-dimensional (1D) DQF sequences, there is no evolution period, $t_1 = 0$, whereas for 2D DQ–SQ experiments, the t_1 delay is incremented. Hence, the evolution of DQC during t_1 is correlated with that of SQC during t_2 and the resulting 2D spectra display DQ–SQ correlations.

γ-Encoded and non-γ-encoded homonuclear dipolar recoupling sequences can be applied during τ periods. When using γ-encoded DQ recoupling, the phase modulation of DQF signal by the angle $2\pi\nu_R t_1$ can be compensated by adjusting the overall rf phase of reconversion sequence [15,34]. This procedure allows varying freely the t_1 period in DQ–SQ experiments and hence the spectral width SW_1 in the indirectly-detected dimension. If the recoupling sequence is non-γ-encoded, a shift in the rf phase does not eliminate the amplitude modulation of the DQF signal by $2\pi\nu_R t_1$. Therefore, the reconversion period must start mandatory an integer number of rotor periods after the end of excitation period. The excitation and reconversion intervals are then said to be rotor-synchronized. As a consequence, in typical 2D DQ–SQ experiments, SW_1 is thus limited to ν_R.

Nevertheless, different methods allow avoiding the signal folding in the F_1 dimension. A first possibility is the use of a shearing transformation with a factor of two in order to convert the DQ–SQ spectrum into a SQ–SQ representation. This shearing transformation reduces the spread in resonance frequencies by a factor of two in the F_1 dimension. In addition, it is possible to scale down along F_1 the isotropic chemical shifts by introducing a π pulse during the evolution of DQC. This variant of DQ–SQ experiment is depicted in Fig. 1b [35]. The π pulse is bracketed by two unequal incremented time periods, qt_1 and $(1-q)t_1$. Therefore, the scaled DQC frequency is $(1–2q)(\nu_j + \nu_k)$, where ν_j and ν_k are the SQ frequencies of the dipolar coupled nuclei, *j* and *k*. For instance, when $q = 1/3$, this method allows reducing the range of ν_{iso} shifts by a factor of 3. The last technique is depicted in Fig. 1c. Prior to the t_1 period, a π pulse refocuses DQC evolution under ν_{iso} shifts during the adjustable delay, 2Γ. The Δt_1 increment time is chosen freely according to the desired spectral width and for each t_1 step, the Γ value is calculated so as to maintain rotor-synchronization of the excitation and reconversion recoupling. In other words, Γ delay is chosen in such way that

$$\tau_\pi + 2\Gamma + t_1 = kT_R \quad \text{with} \quad 0 < \tau_\pi + 2\Gamma \leqslant T_R \quad (6)$$

where τ_π is the length of the π pulse and *k* is an integer. The method described above is derived from that introduced for DQ–SQ experiment using zero-quantum dipolar recoupling [36]. We show that it can be employed for all DQ–SQ sequences incorporating non-γ-encoded recoupling. The pros and the cons of these different techniques to avoid signal folding in the F_1 dimension are discussed in Section 4.

3. Numerical simulations

Numerical simulations were performed to assess the efficiency and the robustness of γ-encoded and non-γ-encoded recoupling sequences at high MAS frequency. These simulations were performed using SIMPSON [37] software for an isolated pair of ^{19}F nuclei denoted I_j and I_k. The inter-nuclear distance was fixed to $d_{jk} = 226$ pm, which corresponds to a dipolar coupling constant $b_{jk}/(2\pi) = -9135$ Hz. We consider two nuclei with either identical chemical shift (Fig. 2a and c) or with two symmetrical chemical shifts with respect to the irradiation frequency ($\nu_{offset} = \Delta\nu_{iso}/2$, Fig. 2b and d). The powder averages were calculated using 320 (α, β) orientations, selected according to the REPULSION algorithm with 15 γ-angles [38]. We detected the magnetization transferred from I_j to I_k during the DQF experiment. It corresponds to one of the two cross-peaks between I_j and I_k transitions on the 2D DQ–SQ spectrum. These simulations were done starting from I_j longitudinal magnetization, i.e. the operator I_{jz}, and detecting only the −1Q coherence of spin I_k, which corresponds to the operator I^-_k. The transferred magnetization was normalized to that of I_k spin after a $\pi/2$ pulse in order to calculate the DQF efficiency. For a spin pair, the above definition results in DQF efficiencies, which are twice smaller than those given by Levitt et al. [16,17].

We performed numerical simulations at various magnetic field strengths and MAS frequencies. In order to simplify the comparison between simulations, the ratio between B_0 and ν_R was kept constant, and the range of ν_{offset} was proportional to B_0. The numerical simulations were thus performed either for (B_0, ν_R) = (9.4 T, 33 kHz) or (18.8 T, 66 kHz).

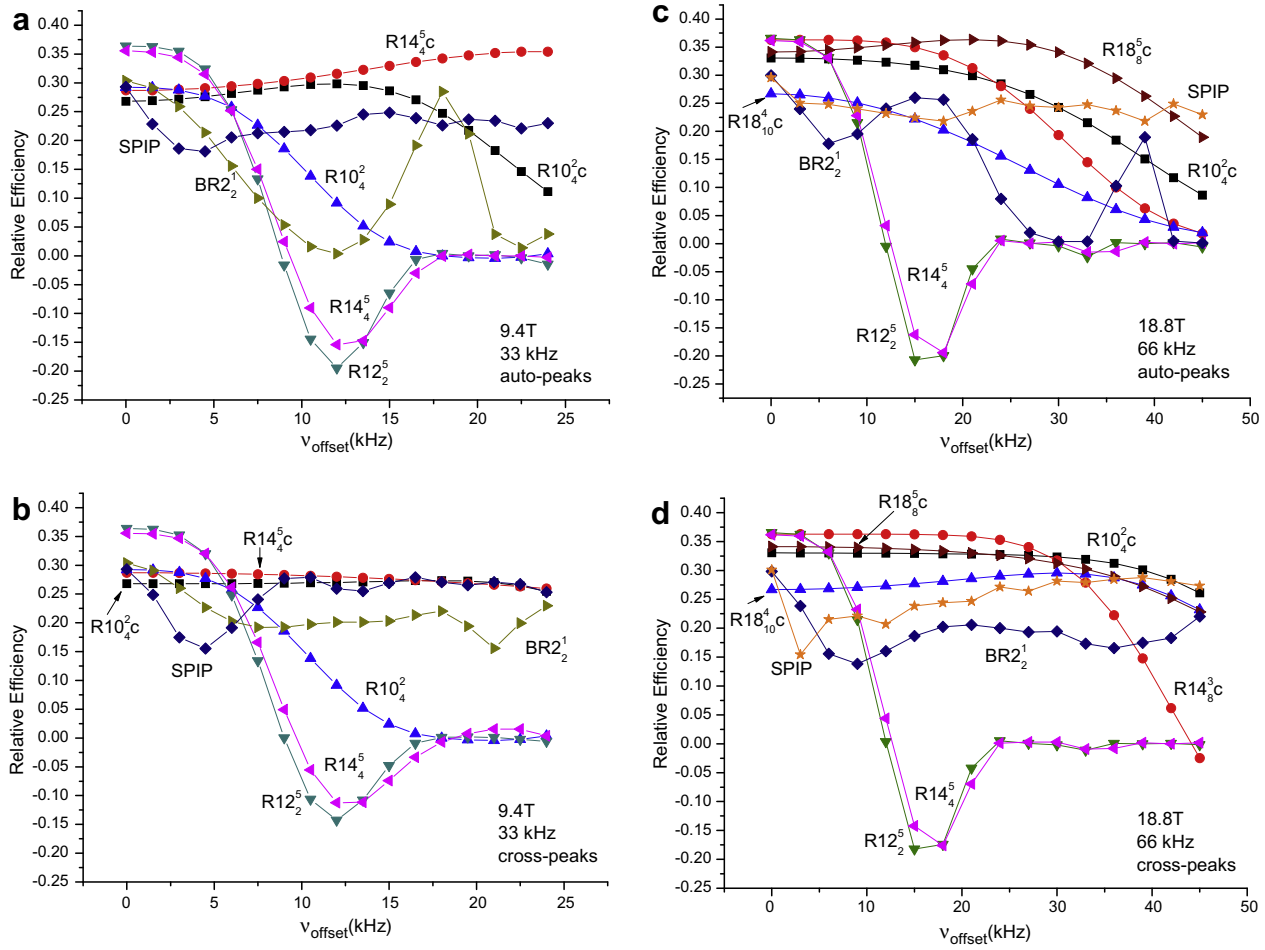

Fig. 2. Numerical simulations of the DQF efficiency versus offset that can be obtained for all allowed sequences, with and without R_4 composite pulse. $b_{jk}/2\pi = -9135$ Hz, CSA = 0. (a and c) auto-peaks, (b and d) cross-peaks with irradiation in the middle of the two peaks: $\nu_{offset} = \Delta\nu_{iso}/2$. (a and b) $\nu_R = 33$ kHz and $B_0 = 9.4$ T (■, $R10_4^2c$; ●, $R14_4^5c$; ▲, $R10_4^2$; ▼, $R12_2^5$; ◀, $R14_4^5$; ▶, $BR2_2^1$; ◆, SPIP; with $\tau = 242, 242, 121, 121, 121, 606, 1212$ μs, respectively). SPIP: $\nu_{1\pi} = 85$ kHz, $\nu_{1SL} = 70$ kHz; $BR2_2^1$: $\nu_{1\pi} = 85$ kHz. (c and d) $\nu_R = 66$ kHz and $B_0 = 18.8$T (■, $R10_4^2c$; ●, $R14_8^3c$; ▲, $R18_{10}^4c$; ▶, $R18_8^5c$; ▼, $R12_2^5$; ◀, $R14_4^5$; ◆, $BR2_2^1$; ★, SPIP; with $\tau = 182, 242, 152, 242, 121, 121, 424, 1333$ μs, respectively). SPIP: $\nu_{1\pi} = 111$ kHz, $\nu_{1SL} = 100$ kHz; $BR2_2^1$: $\nu_{1\pi} = 111$ kHz.

Using numerical simulations, we calculated the DQF efficiency as function of ν_{offset}. We first compared the performances of the basic elements R_1 to R_7 when incorporated into $R14_4^5$, $R10_4^2$, $R14_8^3$, $R18_8^5$ and $R18_{10}^4$ symmetries. The results are presented in the SI. Whatever the RN_n^ν symmetry and the MAS frequency, R_7 composite pulse leads to the highest robustness to offset. However, due to rf limitation, R_7 element can only be used with $R14_8^3$ and $R18_{10}^4$ symmetries. Except R_7, R_4 and R_1 to a lesser extent, are the only composite π pulses which increase the robustness with respect to offsets of nearly all sequences at $\nu_R = 33$ and 66 kHz. This agrees with the prediction of first- and second-order AHT (see Section 2 and Fig. S1). Furthermore, the simulation of DQC build-up curves (not shown) indicates that in the case of ^{19}F–^{19}F distances shorter than 312 pm for one isolated spin pair (i.e. $|b_{jk}|/(2\pi) > 3.5$ kHz), the $R14_8^3$, $R18_8^5$ and $R18_{10}^4$ symmetries cannot be employed at $\nu_R = 33$ kHz, since the maximum of their DQC build-up curves cannot be sampled properly owing to their long cycle time, larger or equal to $8T_R$ (242 μs). This minimum distance is still increased in case of losses and/or three-dimensional ^{19}F networks, as in our test samples. Therefore, at moderate MAS frequency ($\nu_R \approx 30$–35 kHz), it is only useful to analyze the robustness to offset of $R10_4^2$ and $R14_4^5$ γ-encoded sequences with R_1 and R_4 composite π pulses.

In summary, the robustness to offset of all investigated RN_n^ν recoupling sequences can be improved by employing R_1, R_4 or R_7 composite pulses. In the following, we will concentrate on the use of R_4 element, since contrary to R_7, it is compatible with both investigated MAS regimes ($\nu_R \approx 30$ and 65 kHz) and it results in slightly higher robustness to offset and CSA than R_1. In the article, recoupling sequences will be denoted RN_n^ν if they employ a simple 180_0 pulse as basic element and $RN_n^\nu c$ if they employ R_4 composite basic element. With the R_4 composite pulse, the rf amplitude required for the $RN_n^\nu c$ sequences is equal to:

$$\nu_1(R_4) = 7N\nu_R/(6n) \quad (7)$$

Fig. 2 displays the DQF efficiency of diagonal and cross-peaks as function of the carrier frequency offset at $\nu_R = 33$ and 66 kHz. The τ intervals were fixed to the multiple of their cycle time leading to maximal DQF on-resonance efficiency. For $\nu_{offset} = 0$, the DQF efficiencies of γ-encoded sequences $R12_2^5$ and $R14_4^5$ at 9.4 and 18.8 T, and $R14_8^3c$, $R10_4^2c$, and $R18_8^5c$ at 18.8 T, are about the theoretical maximum of 0.365 (i.e. 0.73 using Levitt's convention [16,17]) since the τ delays are close to their optimal values, τ^{opt}, calculated from Eq. (5) (see Table 1). Other on-resonance efficiencies of γ-encoded sequences display lower values owing to the deviation of the delays from τ^{opt}. As expected, the on-resonance efficiencies of non-γ-encoded sequences, SPIP and $BR2_2^1$, are approximately 20% lower than the theoretical maximal efficiency of γ-encoded methods. The long recoupling times employed for SPIP and $BR2_2^1$ sequences are consistent with their small κ_{DD2Q}^{rms} scaling factors (see Table 1).

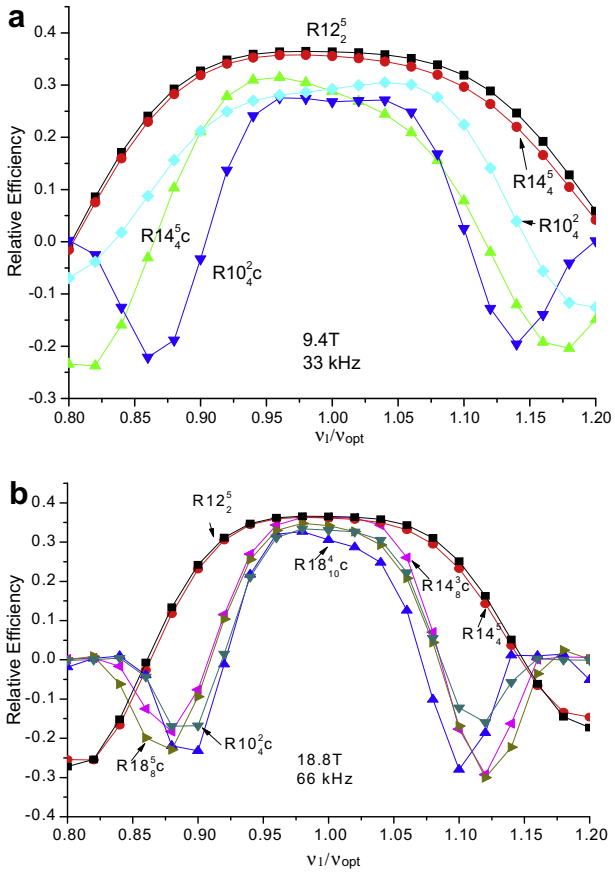

Fig. 3. Numerical simulations of the DQF efficiency versus the deviation in rf nutation frequency for on-resonance auto-peak, for all investigated DQ recoupling sequences, with and without R_4 composite pulse. The nominal rf nutation frequencies are given in Table 1. (a) $\nu_R = 33$ kHz and $B_0 = 9.4$T (■, $R12_2^5$; ●, $R14_4^5$; ▲, $R14_4^5c$; ▼; $R10_4^2c$; ◀, $R10_4^2$; with $\tau = 121, 121, 121, 242, 121$ μs, respectively), (b) $\nu_R = 66$ kHz and $B_0 = 18.8$T (■, $R12_2^5$; ●, $R14_4^5$; ▲, $R18_{10}^4c$; ▶, $R18_8^5c$; ◀, $R14_8^3c$; ▼, $R10_4^2c$; with $\tau = 121, 121, 304, 242, 242, 182$ μs, respectively). $b_{jk}/2\pi = -9135$ Hz. CSA = 0.

These small scaling factors allow sampling properly the maximum of their DQC build-up curves.

Furthermore, the numerical simulations of Fig. 2 permit to assess the robustness to offset of the investigated recoupling methods. The most robust sequences are $R14_4^5c$ and SPIP at $\nu_R = 33$ kHz and $R18_8^5c$ and SPIP at $\nu_R = 66$ kHz. SPIP sequence suppresses offset interferences without the use of composite pulses and hence it benefits from much lower rf-power requirements, especially at $\nu_R = 66$ kHz (Table 1). It must be reminded that none of the composite pulses can be used with $R12_2^5$, which is too much rf demanding.

The improved robustness to offset introduced by the use of composite pulses is partly counter-balanced by the increased sensitivity of these methods to rf-inhomogeneity (Fig. 3). This sensitivity to rf-inhomogeneity can be largely avoided by using restricted samples, at the expense of a decreased signal to noise ratio. This means that composite π pulses, which require larger rf fields than single π pulses, should be used preferentially with samples presenting large chemical-shift ranges.

4. Experimental results

4.1. Samples and experimental conditions

The investigated broadband DQ dipolar recoupling sequences, were tested for three different samples (α-$CaAlF_5$, β-$BaAlF_5$ and $Ba_3Al_2F_{12}$) corresponding to small, moderate and large spreads in ^{19}F chemical shifts, respectively. For ^{19}F sites in these three samples, the magnitudes of anisotropic chemical de-shielding constants ($|\delta_{aniso}|$), determined from spinning sideband patterns, are comprised between 75 and 110 ppm. In this article, the lines (noted L) are numbered starting from the right side of the spectra, and the peaks are described in the figures according to this line notation. We have used the same notation as that used in Ref. [26] to define the fluorine species (noted F). The assignment of the lines has been done for the three samples by simultaneous NMR experiments and DFT calculations [22,26,39]. All inter-nuclear fluorine-fluorine distances up to 375, 473 and 466 pm have been

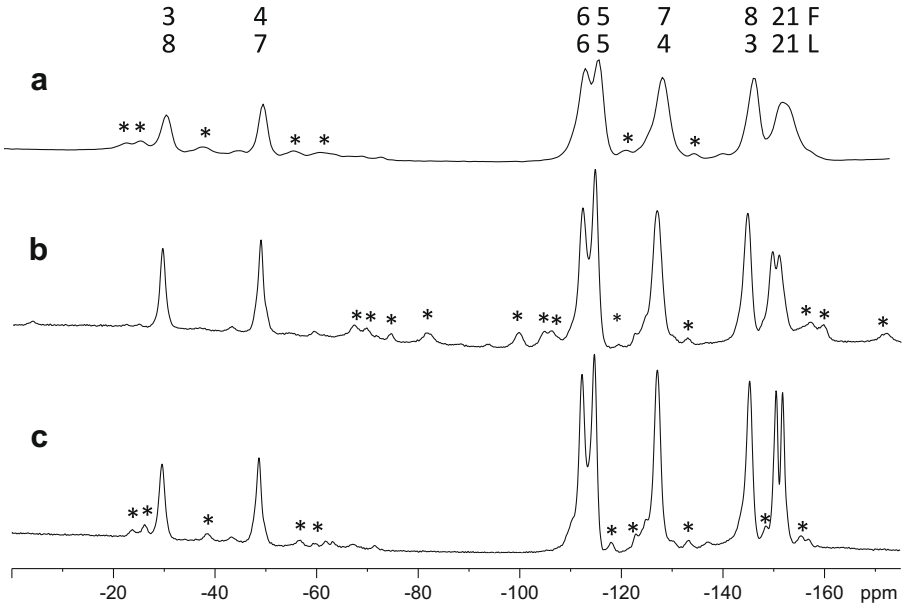

Fig. 4. $Ba_3Al_2F_{12}$. ^{19}F MAS spectra recorded at: (a) 9.4 T and $\nu_R = 30$ kHz, (b) 18.8 T and $\nu_R = 30$ kHz, (c) 18.8 T and $\nu_R = 67$ kHz. The most important spinning sidebands are indicated with ∗.

given for α-$CaAlF_5$, β-$BaAlF_5$ and $Ba_3Al_2F_{12}$, respectively, in the SI of Ref [22].

The structure of α-$CaAlF_5$ is built-up from isolated infinite chains of AlF_6^{3-} octahedra sharing opposite corners [40]. It involves three inequivalent fluorine sites: one shared F1 and two unshared F2 and F3, of multiplicity 4, 8 and 8, respectively. The ^{19}F MAS spectrum exhibits three lines in the small chemical-shift range of $\Delta\delta_{iso}$ = 18 ppm, at −164, −154 and −146 ppm, for L1, L2 and L3, respectively (Fig. S9), with relative intensities 1:2:2. The structure of β-$BaAlF_5$ is built-up from isolated infinite chains of octahedra sharing adjacent corners [41]. This structure involves ten inequivalent sites (two shared F1 and F5, and eight unshared) of same multiplicity. The ^{19}F chemical-shift range of the 10 resonances is moderate: $\Delta\delta_{iso}$ = 55.6 ppm, which means a moderate frequency spread of $\Delta\nu_{iso}$ = 21 kHz at 9.4 T (Fig. 9, Fig. S10). The most difficult sample is $Ba_3Al_2F_{12}$, for which the chemical-shift range is very large and equal to $\Delta\delta_{iso}$ = 122.8 ppm, which represents a large frequency spread of $\Delta\nu_{iso}$ = 46.25 kHz at 9.4 T. The structure of $Ba_3Al_2F_{12}$ is built-up from rings formed by four AlF_6^{3-} octahedra sharing adjacent corners [42]; which involve eight inequivalent F sites: two shared (F1, F2), two free (F3, F4) and four unshared (F5–F8) of multiplicity 4, 4 and 8, respectively (Fig. 4).

All NMR experiments have been performed on Bruker Avance-II spectrometers using wide-bore 9.4 T and narrow-bore 18.8 T magnets. We have employed double resonance MAS probes with rotor o.d. of 1.3 mm at 18.8 T and double or triple resonance MAS probes with o.d. of 2.5 mm at 9.4 T. For all 2D experiments, phase sensitive detection in the indirect dimension was obtained using the States procedure [43]. The ^{19}F chemical shifts were referenced to $CFCl_3$.

The relevance of high magnetic field and high MAS frequency for ^{19}F solid-state NMR is illustrated by Fig. 4. Increases in magnetic field and MAS frequency both contribute to enhance spectral resolution. Large strength of magnetic field spreads the resonance frequencies, when the sample is well crystallized and does not display a continuous distribution of surrounding. High MAS frequencies better average out homogeneous ^{19}F–^{19}F dipolar couplings. For instance, at 18.8 T and ν_R = 67 kHz, the L1 and L2 lines are resolved in the ^{19}F MAS spectrum of $Ba_3Al_2F_{12}$ (see Fig. 4c), whereas

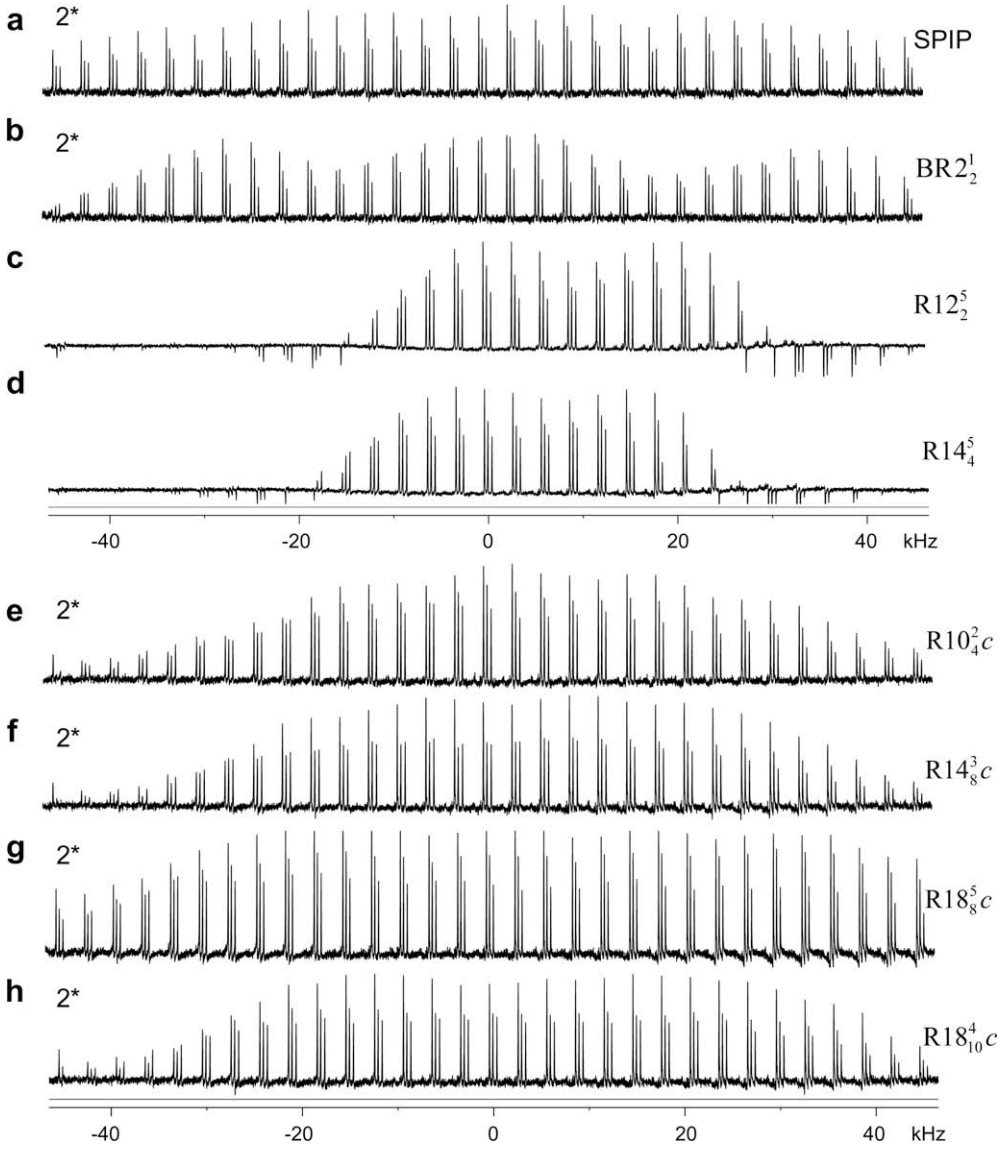

Fig. 5. α-$CaAlF_5$. Experimental DQF spectra versus offset irradiation, recorded at 18.8T and ν_R = 67 kHz. (a) SPIP, (b) BR2$^1_2$, (c) R12$^5_2$, (d) R14$^5_4$, (e) R10^2_4c, (f) R14^3_8c, (g) R18^5_8c, and (h) R18$^4_{10}c$, with τ = 240, 120, 60, 60, 60, 120, 120, 150 μs, respectively. In (e–h) the R_4 composite pulse has been used. All spectra, except those in (c and d) have been scaled up by the factor 2. SPIP: $\nu_{1\pi}$ = 111 kHz, ν_{1SL} = 100 kHz; BR2$^1_2$: $\nu_{1\pi}$ = 111 kHz.

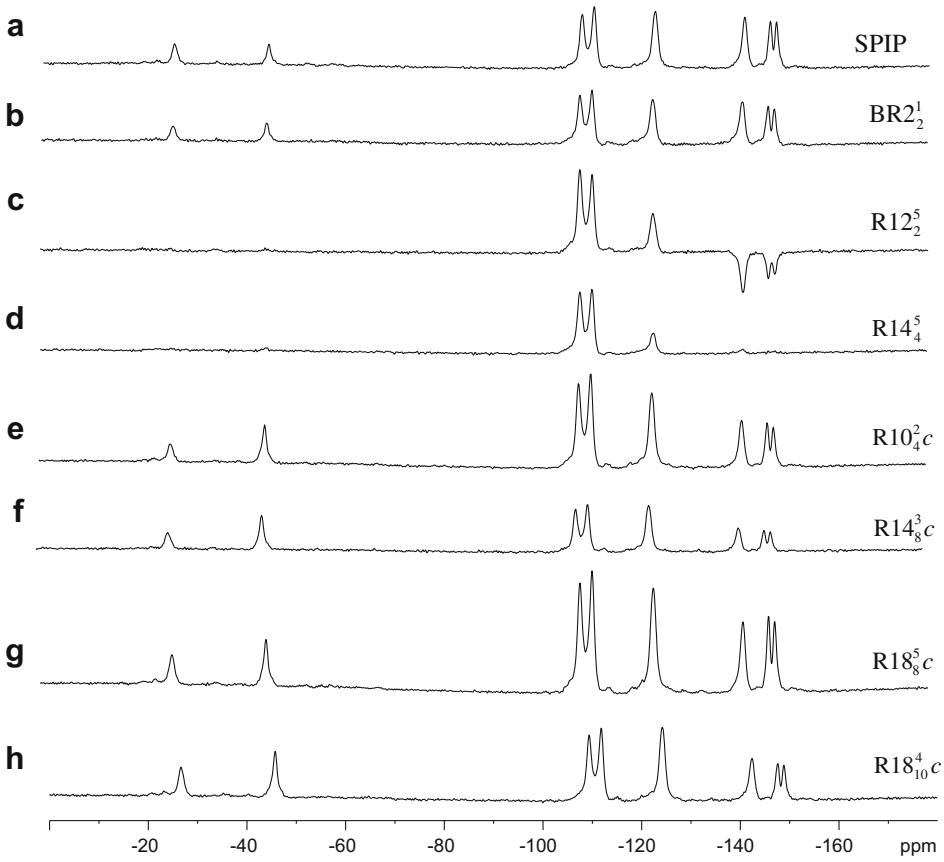

Fig. 6. $Ba_3Al_2F_{12}$. Experimental DQF RN^{ν}_{n} spectra recorded at 18.8 T and ν_R = 67 kHz. (a) SPIP, (b) $BR2^1_2$, (c) $R12^5_2$, (d) $R14^5_4$, (e) $R10^2_4c$, (f) $R14^3_8c$, (g) $R18^5_8c$, and (h) $R18^4_{10}c$, with τ = 240, 120, 60, 60, 60, 120, 120, 150 μs, respectively. In (e–h) the R_4 composite pulse has been used. The rf-irradiation was done at −93 ppm. SPIP: $\nu_{1\pi}$ = 111 kHz, ν_{1SL} = 100 kHz; $BR2^1_2$: $\nu_{1\pi}$ = 111 kHz.

they are not at 9.4 T and ν_R = 30 kHz (see Fig. 4a). A still more advanced solution would be to combine ultra-fast rotation and multiple pulse sequences. This type of homonuclear dipolar decoupling techniques has been developed for protons, which are submitted to small shielding [44–46]. However, the existing decoupling sequences cannot cope with the large shielding of nuclei, such as ^{19}F.

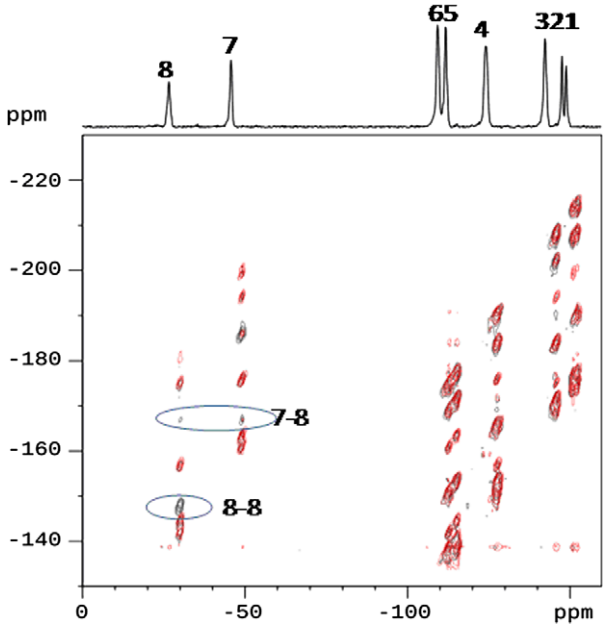

Fig. 7. $Ba_3Al_2F_{12}$. Rotor-synchronized DQ–SQ spectra recorded at 18.8 T and ν_R = 66.6 kHz, with sequence of Fig. 1a. Two recoupling sequences were used: $R18^5_8c$ with R_4 and τ = 120 μs (red) and SPIP with $\nu_{1\pi}$ = 113 kHz, ν_{1SL} = 100 kHz and τ = 180 μs (black). The rf-irradiation was done at −86 ppm. (For interpretation of the references to color in this figure legend, the reader is referred to the web version of this article.)

Besides enhancement in spectral resolution, high MAS frequencies result in longer T'_2 transverse relaxation times [3], larger spectral width in F_1 dimension of rotor-synchronized 2D experiments and larger sampling frequency for the DQC build-up curves. The enhanced resolution observed with high magnetic field and ultra-fast MAS frequency is still emphasized in 2D experiments, and for example it allowed observing relayed negative peaks in the DQ–SQ spectrum of α-$CaAlF_5$ (Fig. S9).

In practice, NMR experiments were performed either at (B_0, ν_R) = (9.4 T, 30–32 kHz) or (18.8 T, 65–67 kHz). For both experimental conditions, the ratio between CSA magnitude and MAS frequency is approximately constant and identical numbers of CSA spinning sidebands are observed in the NMR spectra. The only difference between the two series of experiments lies in the magnitude of offset and effective homonuclear dipolar couplings.

4.2. DQF efficiency and robustness to offset

In Fig. 5 are represented the DQF signals of α-$CaAlF_5$ recorded versus offset (−45 to 45 kHz) at B_0 = 18.8 T and ν_R = 67 kHz. At this field, the chemical frequency range of this sample is moderate ($\Delta\nu_{iso}$ = 13.6 kHz) and the behaviors of the three lines are globally identical. Fig. 5 allows assessing the robustness to offset of the different investigated recoupling sequences compatible with ν_R = 67 kHz. In agreement with numerical simulations, the γ-encoded $R12^5_2$ and $R14^5_4$ sequences result in the largest on-resonance sensitivity. The other γ-encoded recoupling methods, $R10^2_4c$, $R14^3_8c$, $R18^5_8c$ and $R18^4_{10}c$,

provide lower DQF efficiency. First, these sensitivity decreases stem from their smaller κ^{rms}_{DD2Q} values (Table 1), which lead to longer optimum recoupling times τ^{opt} and thus larger losses. The contact time used for $R10^2_4c$ was smaller than its optimum value. Second, owing to their large cycle times ($\geqslant 4T_R$), the maximum of DQC build-up curves cannot be sampled properly. The on-resonance DQF efficiencies of non-γ-encoded SPIP and $BR2^1_2$ sequences are comparable with those of $RN^\nu_n c$ schemes. However, the main differences between all these sequences lie in their robustness to offset. The γ-encoded $R12^5_2$ and $R14^5_4$ sequences built from $R = 180_0$ element are quite sensitive to offset. They can only be employed in the case of nuclei with limited $\Delta\nu_{iso}$ range, such as ^{1}H [18]. Whereas the schemes displaying highest robustness are SPIP and $R18^5_8c$, and $BR2^1_2$ to a lesser extent. For very large offsets, SPIP and $R18^5_8c$ provide approximately the same DQF efficiency. However, the rf-power requirement of SPIP is 2.9 lower than that of $R18^5_8c$ (Table 1).

The key advantage of high robustness to offset for ^{19}F solid-state NMR is illustrated by the DQF spectra of $Ba_3Al_2F_{12}$ at 18.8 T and $\nu_R = 67$ kHz (Fig. 6). The limited robustness of $R12^5_2$ and $R14^5_4$ sequences does not allow the simultaneous excitation of DQC for shielded and de-shielded ^{19}F resonances. The other recoupling techniques allow obtaining significant simultaneous DQF signals for resonances separated by 92.5 kHz. The $R18^5_8c$ recoupling sequence benefits from the highest on-resonance efficiency. However, the variation of DQF efficiency with offset for this sequence modifies the relative intensity of the ^{19}F lines. Such an effect is less pronounced in the case of SPIP. The very good robustness of SPIP with respect to offset has also been observed in the DQF spectra of β-$BaAlF_5$ recorded at 9.4 T with $\nu_R = 30$ kHz (Fig. S10).

The higher robustness to offset of SPIP compared to $R18^5_8c$ was confirmed by recording at 18.8 T and $\nu_R = 66.6$ kHz the ^{19}F DQ–SQ spectra of $Ba_3Al_2F_{12}$ with either SPIP or $R18^5_8c$ as recoupling sequence (Fig. 7). In order to limit the differences between the two experiments, the excitation and reconversion recoupling intervals were rotor-synchronized for both γ-encoded and non-γ-encoded recoupling schemes. SPIP sequence allowed the observation of auto-peak L8–L8 and cross-peak L7–L8 between de-shielded resonances, whereas these correlations are missing in the 2D spectrum obtained by using $R18^5_8c$.

We also investigated the robustness to offset of DQ recoupling sequences at $\nu_R = 30$ kHz with $B_0 = 9.4$ T. Fig. 8 displays the DQF efficiency of α-$CaAlF_5$ as function of the offset. The highest on-resonance DQF efficiency is obtained for $R12^5_2$ sequence. The losses and the numerous homonuclear dipolar couplings lead to an optimal recoupling time, approximately divided by two compared to the numerical simulations of Fig. 2 for an isolated spin pair. The lower DQF efficiency of $R14^5_4$ arises from its longer cycle time and its large κ^{rms}_{DD2Q} scaling factor, which prevent from reaching the maximal DQF efficiency. Owing to its smaller κ^{rms}_{DD2Q} scaling factor, $R14^5_4c$ method provides on-resonance sensitivity close to that of $R12^5_2$. The non-γ-encoded sequences SPIP and $BR2^1_2$ display on-resonance DQF efficiencies lower than $R12^5_2$ and $R14^5_4c$. It must be noted that the $BR2^1_2$ sequence is more modulated by the offset at 9.4 T than at 18.8 T (compare Fig. 5b and Fig. 8b). At $\nu_R = 30$ kHz, the highest robustness to offset is obtained for SPIP and $R14^5_4c$. The $R14^5_4c$ sequence benefits from higher on-resonance sensitivity but requires 2.8 times larger rf-power than SPIP (Table 1).

4.3. Avoiding signal folding in the F_1 dimension

Fig. 9 displays two HOMCOR spectra of β-$BaAlF_5$ recorded at 9.4 T and $\nu_R = 30$ kHz. The SPIP scheme was employed as recoupling method in the pulse sequence of Fig. 1a and, as SPIP is not

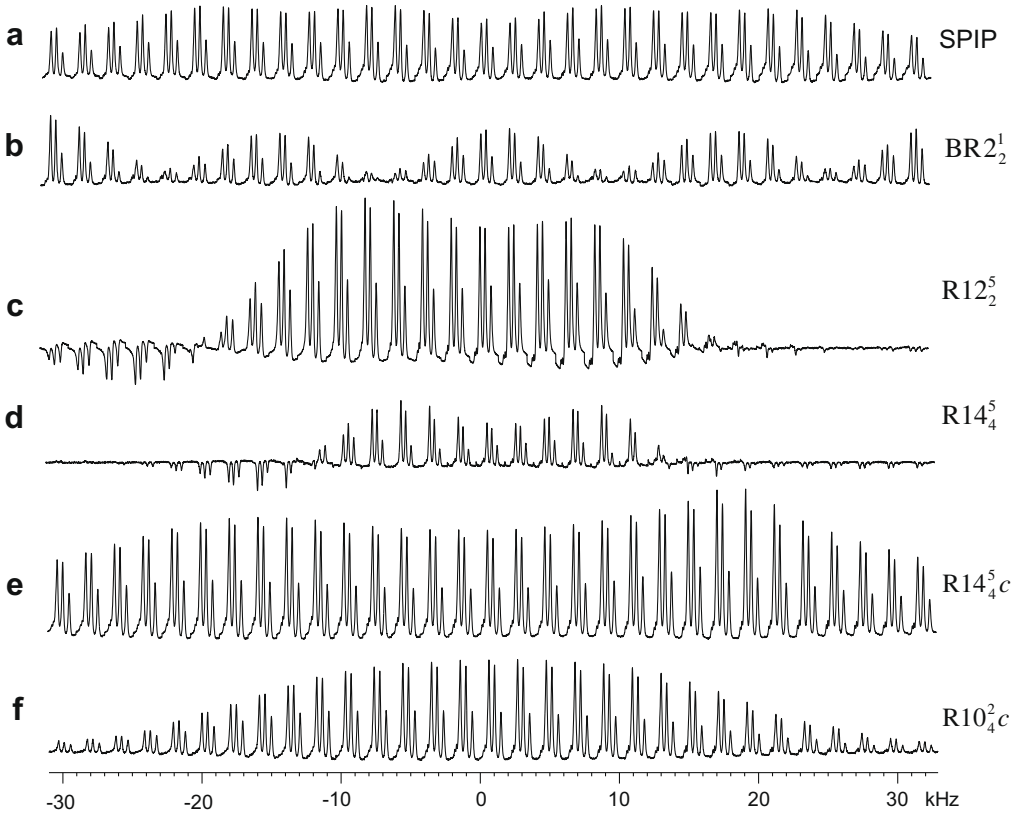

Fig. 8. α-$CaAlF_5$. 1D ^{19}F experimental DQF spectra versus offset (−30 to 30 kHz) at 9.4 T with $\nu_R = 30$ kHz. The DQ recoupling schemes are (a) SPIP, (b) $BR2^1_2$, (c) $R12^5_2$, (d) $R14^5_4$, (e) $R14^5_4c$, and (f) $R10^2_4c$, with $\tau = 266.7, 133.3, 66.7, 133.3, 133.3, 133.3$ μs, respectively. The other sequences, $R18^5_8$, $R14^3_8$, $R18^4_{10}$, $R18^5_8c$, $R14^3_8c$, and $R18^4_{10}c$, could not be optimized correctly owing to too long recoupling periods ($8T_R$ or $10T_R$). SPIP: $\nu_{1\pi} = 85$ kHz, $\nu_{1SL} = 78$ kHz; $BR2^1_2$: $\nu_{1\pi} = 85$ kHz. $RN^\nu_n c$ sequences have used R_4 composite pulses.

γ-encoded, the excitation and reconversion intervals were rotor-synchronized. Therefore, the spectral width in the F_1 dimension is limited to $SW_1 = \nu_R$. Even if the chemical-shift range $\Delta\delta_{iso}$ = 55.6 ppm, and the strength of magnetic field are moderate, the spread in resonance frequencies of DQC reaches 42 kHz and thus exceeds $SW_1 = \nu_R$. Consequently, in the usual DQ–SQ representation (shown in Fig. 9a), six peaks are folded along F_1: L1–L1, L1–L2, L1–L3, L2–L3, L9–L10, and L10–L10. However, as in that case the spread in resonance frequencies of SQC, $\Delta\nu_{iso}$ = 21 kHz is lower than ν_R, this signal folding can be avoided by doing a shearing processing with a factor of two. After such a shearing, the slope of the auto-peaks becomes equal to one, and the spectrum is then presented in a symmetrical way (Fig. 9b), as a SQ–SQ spectrum. However, this shearing is useless when $\Delta\nu_{iso}$ is larger than ν_R. This is illustrated by the 2D $^{19}F-^{19}F$ HOMCOR spectra of $Ba_3Al_2F_{12}$ at 9.4 T, for which the frequency spread ($\Delta\nu_{iso}$ = 46.25 kHz) is larger

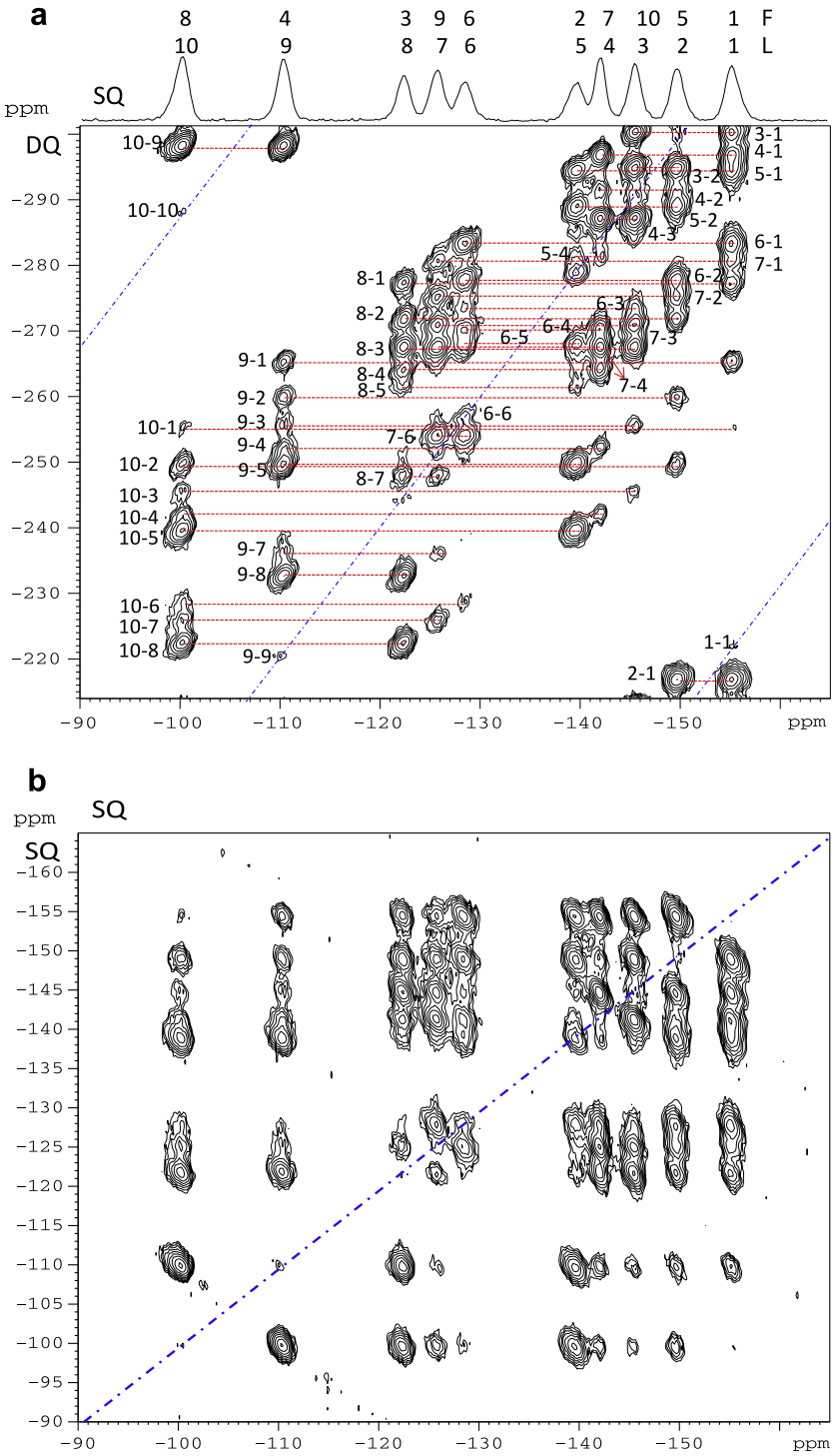

Fig. 9. β-$BaAlF_5$. Experimental SPIP DQ-SQ spectrum recorded at 9.4 T with ν_R = 30 kHz and the sequence of Fig. 1a. The rf-irradiation was done at −129 ppm. The nutation frequencies of SPIP were: $\nu_{1\pi}$ = 85 kHz, ν_{1SL} = 78 kHz, and τ = 267 μs. (a) Un-sheared spectrum. Due to the folding along F_1, the vertical scaling is only correct for the central part of the resonances. For the four other resonances, the correct F_1 value can be obtained by adding either + 80 ppm for (10, 10) and (10, 9), or −80 ppm for (2, 1) and (1, 1) correlation peaks (80 ppm = ν_R/ν_0). (b) Sheared spectrum; the vertical scaling is correct for all peaks.

than ν_R = 30 kHz (Fig. 10). Indeed, the sheared spectrum shown in Fig. 10b is much more difficult to interpret than that shown in Fig. 10a. The only difference with respect to the un-sheared spectrum recorded with a sufficient spinning speed ($\nu_R > 2\Delta\nu_{iso}$) is that the auto-correlation line is parted in several pieces of lines in Fig. 10a.

For samples with large spread in resonance frequencies ($\Delta\nu_{iso} > \nu_R$), the signal folding in F_1 dimension for non-γ-encoded recoupling schemes can be avoided by inserting a π pulse during the evolution period of DQC (Fig. 1b and c). However, when the delays between central π pulse and the recoupling intervals are not multiple of the rotor period, this π pulse reintroduces the CSA during one rotor period at the maximum. This unwanted dephasing may be non negligible in case of large CSA, as with ^{19}F nuclei. Fig. 11 shows that the non-refocused CSA affects the sensitivity of DQF experiments. The variation in DQF efficiency with the de-synchronization delay Γ differs

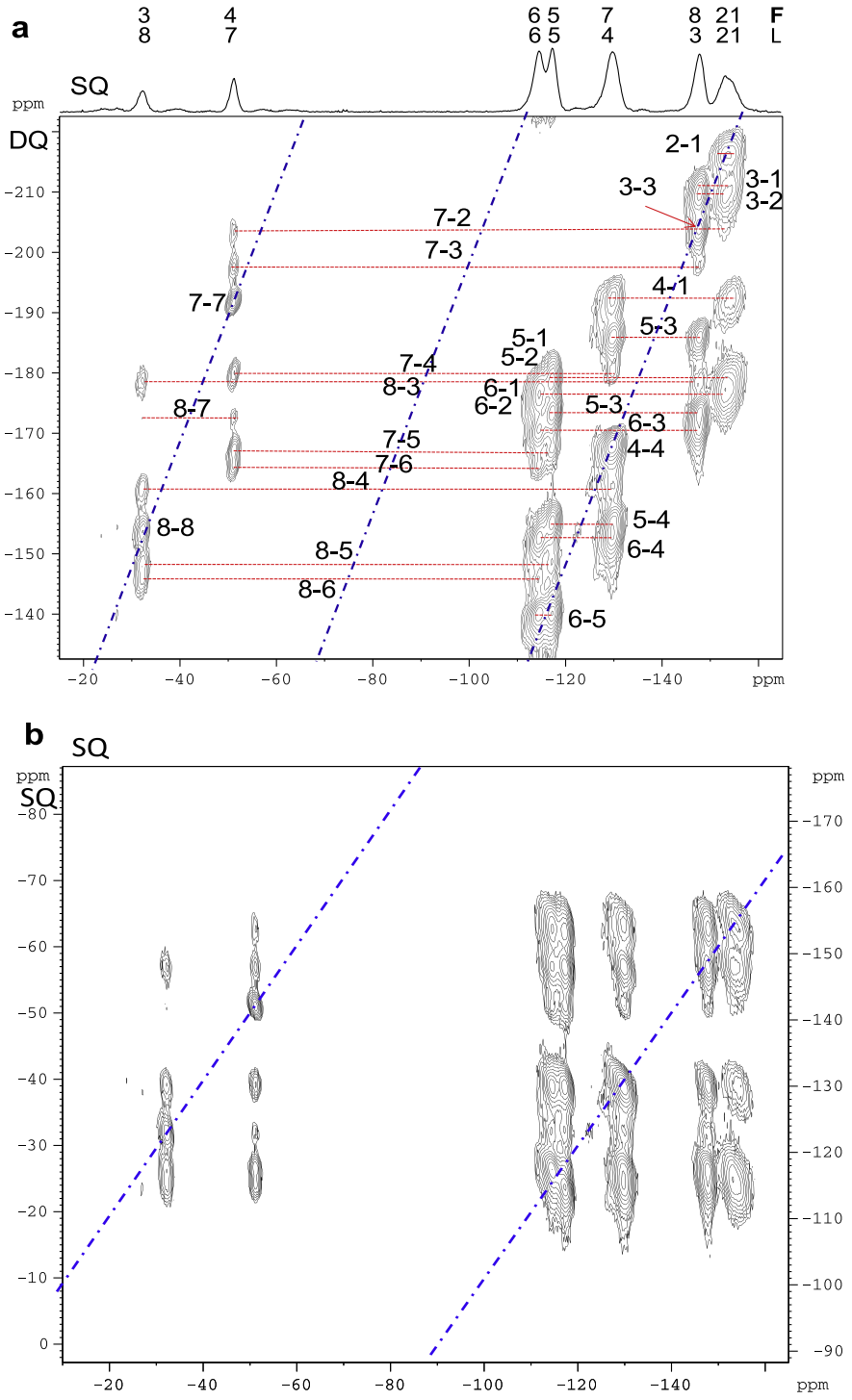

Fig. 10. $Ba_3Al_2F_{12}$. Experimental 2D SPIP DQ–SQ spectrum recorded at 9.4 T with ν_R = 30 kHz and the sequence of Fig. 1a. The nutation frequencies of SPIP were: $\nu_{1\pi}$ = 85 kHz, ν_{1SL} = 78 kHz, and τ = 267 μs. The rf-irradiation was done at −93 ppm. (a) Un-sheared spectrum. Due to the folding along F_1, the vertical scaling is only correct for the central part of the resonances. For the other resonances, the correct F_1 value can be obtained by adding ±80 ppm (80 ppm = ν_R/ν_0). (b) Sheared spectrum. The right (resp. left) vertical scaling concerns the right (resp. left) peaks.

between $BR2_2^1$ and SPIP. As the spin dynamics created by first-order AH terms is identical with $BR2_2^1$ and SPIP recoupling, the discrepancy in DQF efficiencies for de-synchronized π pulse must arise from different recoupled CSA terms in the second-order AH. This is supported by the fact that $BR2_2^1$ sequence is more robust to CSA than SPIP [20]. Fig. 11 demonstrates that practically $BR2_2^1$ scheme has to be preferred over SPIP for the pulse sequences of Fig. 1b and c.

The DQ–SQ experiments of Fig. 1b and c were compared with $SW_1 = 3\nu_R$ in the case of $Ba_3Al_2F_{12}$ at 9.4 T and $\nu_R = 30$ kHz (Fig. 12). Both methods allow avoiding signal folding in F_1 dimension. The method of Fig. 1b scales the chemical shifts along F_1 by the factor $(1 - 2q)$. The total evolution time on DQC must thus be $(1 - 2q)$ times longer than that related to methods described in Fig. 1a and c, to observe the same resolution. However, the homogeneous line broadening is not affected by the central π pulse and this longer evolution time on DQC thus leads to a decreased resolution. This effect can be observed by comparing spectra shown in Fig. 12a and b and recorded with methods described in Fig. 1b and c, respectively.

An alternative to the method of Fig. 1c consists in incorporating γ-encoded recoupling schemes in the pulse sequence of Fig. 1a. For instance, the $R14_4^5c$ sequence was used at $\nu_R = 30$ kHz to acquire the DQ–SQ spectrum of $Ba_3Al_2F_{12}$ (Fig. 12c). The increment $\Delta t_1 = T_R/3$ allowed avoiding the signal folding along the F_1 dimension and the spectral resolution was similar to that of Fig. 12b. However, spinning sidebands along F_1 dimension appeared. These sidebands always exist in case of large CSA and non rotor-synchronized excitation and reconversion recoupling. Their intensities depend on the recoupling sequence, and as an example, they are larger with the $R14_4^5c$ sequence than with the $BR2_2^1$ sequence (compare Fig. 12b and c).

Experiments similar to those of Fig. 12b and c were performed at 18.8 T and $\nu_R = 65$ kHz, with $SW_1 = 3\nu_R$. The γ-encoded and non-γ-encoded recoupling schemes were $R18_8^5c$ and $BR2_2^1$, with the pulse sequences of Fig. 1a and c, respectively. The corresponding 2D spectra, presented in Fig. 13a and b, show that DQ–SQ spectra without any signal folding can be acquired even if the spread in resonance frequencies of DQC covers 185 kHz. Compared to Fig. 12c, the spectrum of Fig. 13a displays a larger number of CSA spinning sidebands owing to the different recoupling sequence. These spinning sidebands complicate the spectrum analysis. The intensity of these sidebands is much lower when using $BR2_2^1$ recoupling (compare Fig. 13a and b-1). The spectrum of Fig. 13b can be compared with that of Fig. 13c, which was obtained by using SPIP recoupling incorporated into the pulse sequence of Fig. 1a. The spectrum of Fig. 13b benefits from the absence of signal folding along the F_1 dimension. However, the rotor-synchronized SPIP sequence is more robust to offset than the non-rotor-synchronized $BR2_2^1$. Consequently, the L1–L1, L8–L3 and L4–L2 correlations can be easily observed in Fig. 13c but not in Fig. 13b. Furthermore, the 2D spectrum of Fig. 13c was acquired in three-times less experimental time than that of Fig. 13b.

5. Conclusions

We have presented, analyzed and compared several homonuclear dipolar double-quantum recoupling methods for nuclei submitted to large homonuclear dipolar interactions, such as ^1H and ^{19}F. These rotor-synchronized and symmetry-based methods are the non-γ-encoded SPIP and $BR2_2^1$ sequences, and several γ-encoded RN_n^ν sequences. The main criteria of choice are related to: (1) the spinning speed, (2) the rf-power limitation of the probe,

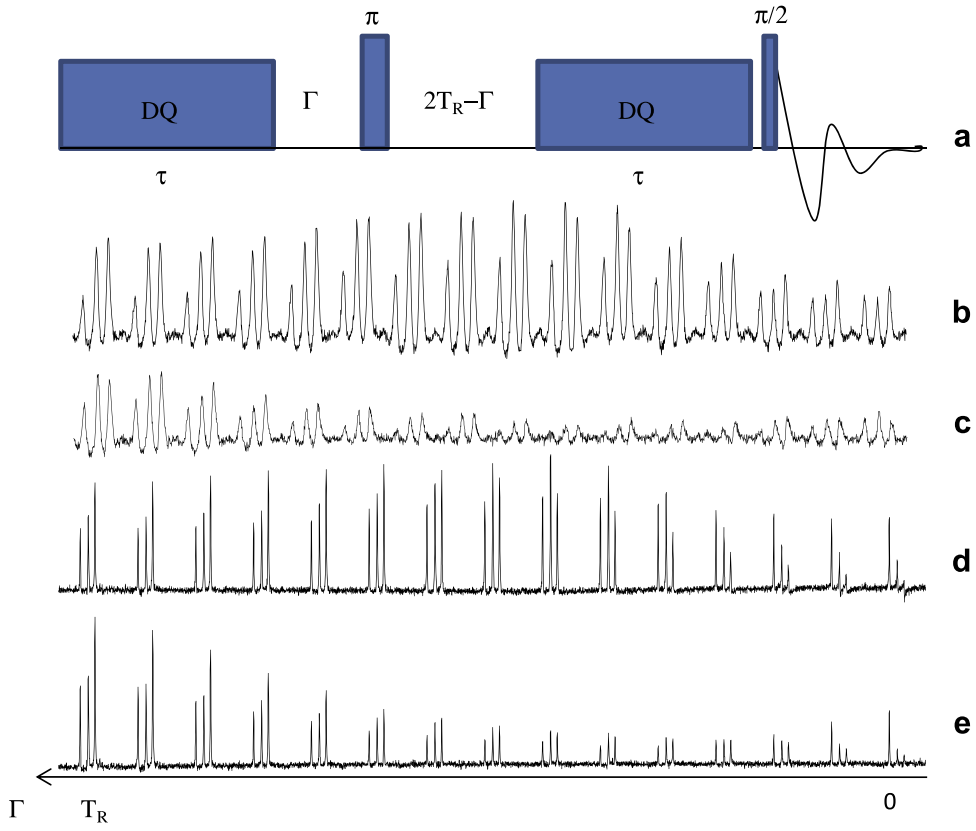

Fig. 11. Effect of an additional π pulse on 1D DQF spectra of α-$CaAlF_5$ at: (b and c) $B_0 = 9.4$ T and $\nu_R = 32$ kHz or (d and e) $B_0 = 18.8$ T and $\nu_R = 60$ kHz. The DQF signals were acquired by employing the pulse sequence depicted in (a) using non-γ-encoded schemes: $BR2_2^1$ in (b and d) and SPIP in (c and e). The delay Γ was varied from 0 to T_R. At $\Gamma = T_R$, the CSA is refocused. SPIP: $\nu_{1\pi} = 105$ kHz, $\nu_{1SL} = 97$ kHz, $\tau = 266.7$ μs; $BR2_2^1$: $\nu_{1\pi} = 105$ kHz, $\tau = 133.3$ μs.

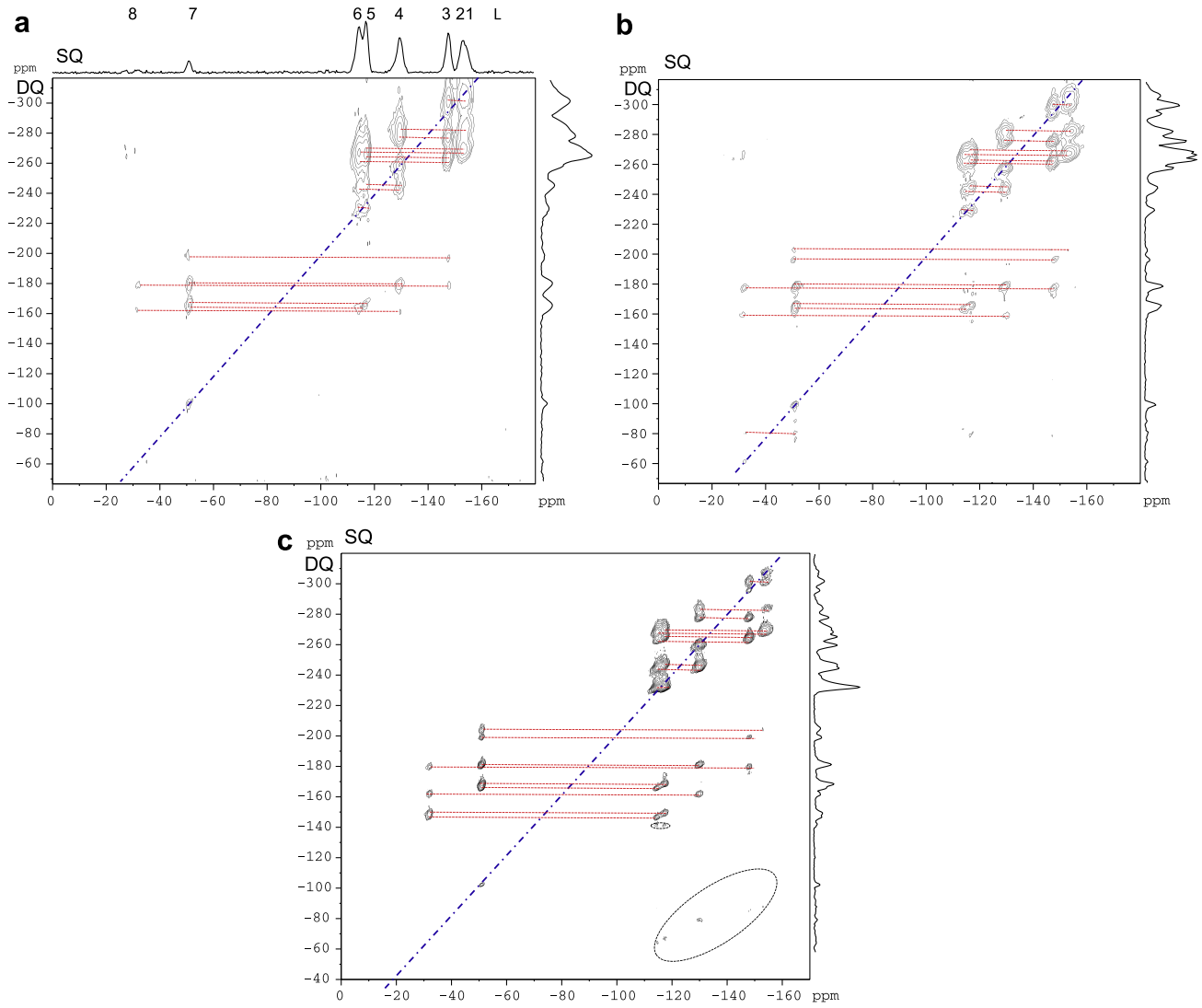

Fig. 12. $Ba_3Al_2F_{12}$. Experimental DQ–SQ un-sheared spectra recorded at 9.4 T with ν_R = 30 kHz and the same spectral width of $SW_1 = 3\nu_R$. (a and b) Spectra obtained with $BR2_2^1$ and the pulse sequence described either: (a) in Fig. 1b with $\Delta t_1 = T_R$ and $q = 1/3$; the spectrum has been re-scaled along F_1 or (b) in Fig. 1c with $\Delta t_1 = T_R/3$. (c) Spectrum recorded with $R14_4^5c$ sequence with R_4 and the pulse sequence described in Fig. 1a and $\Delta t_1 = T_R/3$. Regions which are circled in (c) are small sidebands along F_1 of the cross-peaks. They are hardly observable in (a and b). $BR2_2^1$: $\nu_{1\pi}$ = 85 kHz, τ = 133.3 μs. $R14_4^5c$: τ = 133.3 μs.

(3) the spread in resonance frequency $\Delta\nu_{iso}$, (4) the optimum recoupling time (for loss reasons) and (5) the requirement of high sensitivity. It must be noted that ^1H and ^{19}F are two very NMR sensitive nuclei, and that the on-resonance sensitivity of the methods is thus generally not the main criterion of choice.

When the frequency range is small, $\Delta\nu_{iso} < 0.5\nu_R$, such as ^{19}F in α-$CaAlF_5$ or ^1H in general, there is no offset limitation. The criteria of choice in between SPIP, $BR2_2^1$, $R12_2^5$, $R14_4^5$, $R10_4^2$, $R14_8^3$, $R18_8^5$, and $R18_{10}^4$ sequences are thus only related to the required rf field and the optimum recoupling time. $R12_2^5$, which benefits from a small cycle ($2T_R$) and a short optimum recoupling time, thus leading to easy sampling of the built-up curve and weak losses, is the sequence of choice if the probe can provide a sufficient rf field, especially at ultra-fast MAS ($\nu_1 = 3\nu_R$). Furthermore, it benefits from larger DQF efficiency than SPIP. If $R12_2^5$ is not compatible with the rf-power limitation of the probe, alternatives consist in using SPIP or $R14_4^5$. However, SPIP should then be preferred owing to its shorter cycle time ($2T_R$) and smaller required rf-field, especially at ultra-fast MAS.

When the frequency range is moderate, $0.5\nu_R < \Delta\nu_{iso} < \nu_R$, such as ^{19}F in β-$BaAlF_5$, the sequence must be selected according to the same previous criteria, but a shearing processing by a factor of two may be used to avoid the folding of the resonances along F_1.

When the frequency range is large, $\Delta\nu_{iso} > \nu_R$, such as ^{19}F in $Ba_3Al_2F_{12}$, γ-encoded sequences, such as $R12_2^5$, built from single 180_0 pulse have a too limited offset robustness. A possible solution consists in employing broadband composite π pulses (e.g. R_4: $60_0300_{180}60_0$) as basic element. This method enhances the robustness to offsets of RN_n^ν sequences but also their rf requirement. We show that $R14_4^5c$ and $R18_8^5c$ recoupling methods allow acquiring DQ–SQ spectra of $Ba_3Al_2F_{12}$ at $\nu_R \approx 30$ and 65 kHz, respectively. If these γ-encoded methods allow avoiding the signal folding, they create significant spinning sidebands along F_1 dimension. The DQ–SQ spectra of $Ba_3Al_2F_{12}$ can also be obtained by using non-γ-encoded methods, such as SPIP and $BR2_2^1$. The introduction of a π pulse during the evolution period of DQC allows avoiding the signal folding. In that case, we show that $BR2_2^1$ has to be employed. The 2D spectra acquired by this method display small spinning sidebands, which simplify the spectral interpretation. Finally the super-cycled SPIP sequence benefits from the highest robustness to offset and allows the observation of homonuclear correlation between sites displaying large differences in isotropic chemical shifts.

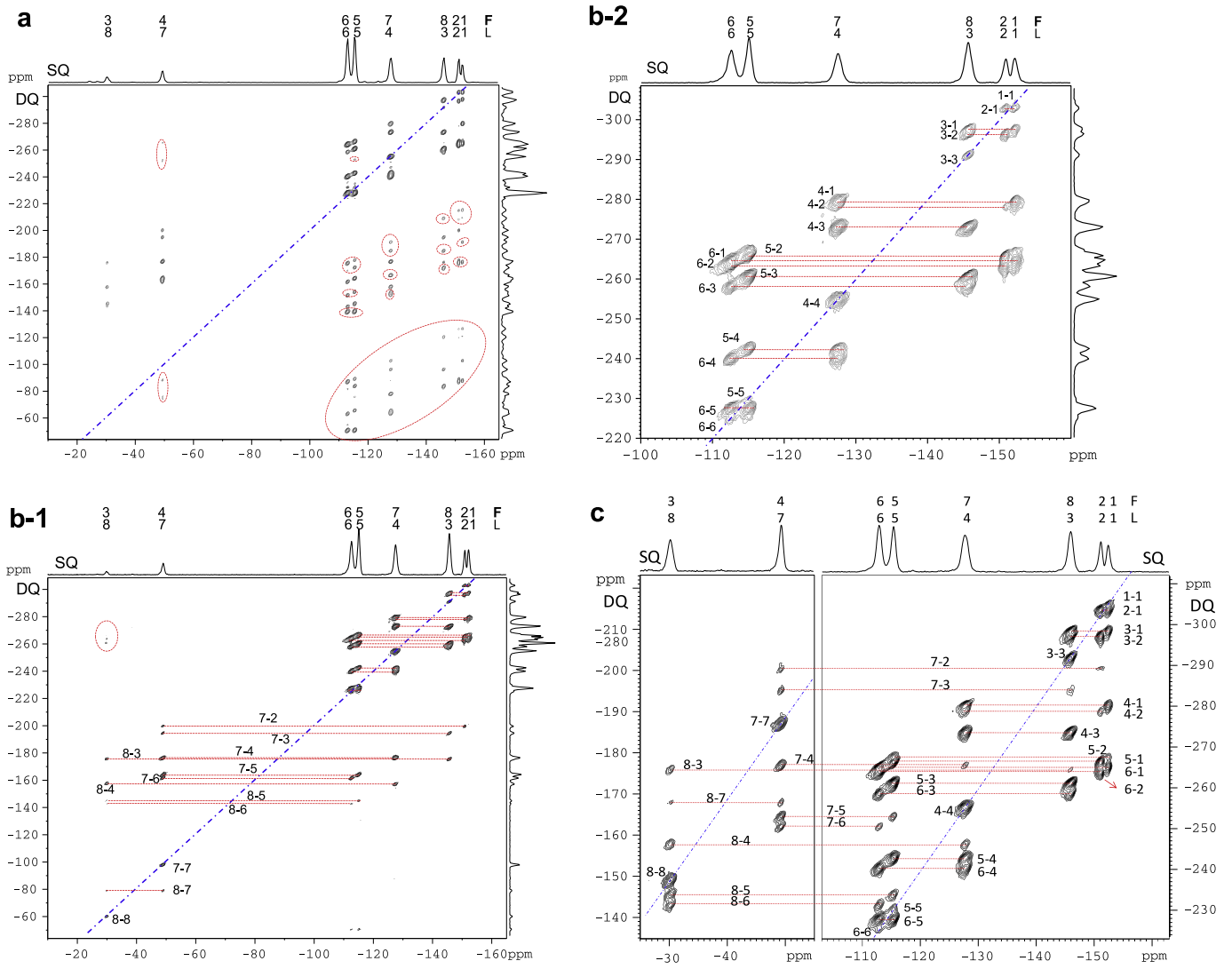

Fig. 13. $Ba_3Al_2F_{12}$. DQ–SQ spectra recorded at 18.8 T with ν_R = 65 kHz and the rf-irradiation at −93 ppm. Two recoupling schemes were used with same $SW_1 = 3\nu_R$ ($\Delta t_1 = T_R/3$): (a) $R18_8^5c$ with R_4 and sequence of Fig. 1a (τ = 120 μs), and (b-1) $BR2_2^1$ with sequence of Fig. 1c (τ = 120 μs and $\nu_{1\pi}$ = 120 kHz). (b-2) Expansion of the right upper part of (b-1), in order to obtain the same spectral widths as the right part of (c). (c) Rotor-synchronized ($SW_1 = \nu_R$) SPIP spectrum with: $\nu_{1\pi}$ = 120 kHz, ν_{1SL} = 100 kHz, and τ = 240 μs. The full spectrum has been acquired in a single experiment but for the sake of readability, only the spectral regions displaying correlation peaks are presented. Due to the folding along F_1, the vertical scaling on the right is only correct for the pairs of correlation peaks both situated in the right square of the spectrum. The vertical scaling on the left, which is correct for the pairs of correlation peaks with one peak in the left part and one peak in the right part, has been obtained by adding 86.3 ppm (ν_R/ν_0) to the right vertical scaling. For the three other peaks ((8, 8), (8, 7), (7, 7)), the correct F_1 value can be obtained by adding 86.3 ppm to this left vertical scaling.

As SPIP scheme is not compatible with the introduction of a central π pulse, the absence of signal folding has to be sacrificed for the sake of greater robustness. In summary, in the case of very large frequency spread for the resonances, our preferred choice is to introduce rotor-synchronized SPIP recoupling into the usual DQ–SQ experiment (Fig. 1a). This method provides the highest robustness to offset, requires low rf field, minimizes the experimental time and eliminates sidebands along the F_1 dimension. If the interpretation of the SPIP DQ–SQ spectrum with folded peaks appears difficult to the scientist, our second choice is then the non-rotor-synchronized $BR2_2^1$ scheme with a π pulse during the evolution period. Folded resonances along F_1 are avoided, but the sensitivity is largely decreased with respect to rotor-synchronized SPIP.

It must be noted that experimental relative efficiencies of the various sequences do not always correspond to those obtained with simulations. These differences of relative efficiencies are related to the sparse sampling of the built-up curves and to the irreversible losses. Practically, the best way to sample correctly the built-up curves may thus be: first to find with a fast spinning speed the best number of recoupling cycles, and second to optimize the spinning speed, while keeping the same number of cycles. Obviously, these problems of sparse sampling and irreversible losses decrease with increasing field and spinning speed.

It is also very important to note the great advantage of using the highest available spinning speed and magnetic field for resolution purpose. The use of small sample volumes for ultra-fast spinning speed is indeed most of the time not a problem for these very sensitive nuclei.

Last, it must be reminded that all double- and zero-quantum dipolar recoupling sequences intrinsically suffer from dipolar truncation effects [47,48] meaning that medium- or long-range spatial proximities between two nuclei cannot be directly probed when one of these is also involved in a short-range correlation with a third nucleus. However, this important limitation may be now partly overcome by some new advanced recoupling methods [49,50].

Acknowledgments

Authors are grateful for funding provided by Region Nord/Pas de Calais, Europe (FEDER), CNRS, French Minister of Science, USTL, ENSCL and Bruker BIOSPIN. They also thank Drs. F. Fayon and F. Aussenac for helpful discussions and Drs. A. Le Bail, A.M. Mercier, and M. Body, who supplied the samples. Financial support from the TGE RMN THC (FR-3050) for conducting the research is gratefully acknowledged. They also would like to thank Prof. Malcolm H. Levitt and Dr. Andreas Brinkmann for providing the 'C and R symmetries' Mathematica package. F.D. thanks the National Natural Science Foundation of China (20773159, 20673139, 20933009) and the National Basic Research Program of China (2009CB918600) for financial support.

Appendix A. Supplementary data

Supplementary data associated with this article can be found, in the online version, at doi:10.1016/j.jmr.2009.12.009.

References

[1] A. Samoson, Extended magic-angle spinning, in: D.M. Grant, R.K. Harris (Eds.), Encyclopedia of Nuclear Magnetic Resonance, vol. 9, John Wiley & Sons, Chichester, 2002, pp. 59–64.
[2] L.S. Du, A. Samoson, T. Tuherm, C.P. Grey, $^{19}F/^{23}Na$ double resonance MAS NMR study of oxygen/fluorine ordering in the oxyfluoride $Na_5W_3O_9F_5$, Chem. Mater. 12 (2000) 3611–3616.
[3] [a] K. Mao, J.W. Wiench, V.S.Y. Lin, M. Pruski, Indirectly detected through-bond chemical shift correlation NMR spectroscopy in solids under fast MAS: studies of organic-inorganic hybrid materials, J. Magn. Reson. 196 (2009) 92–95;
[b] K. Mao, M. Pruski, Directly and indirectly detected through-bond heteronuclear correlation solid-state NMR spectroscopy under fast MAS, J. Magn. Reson. 201 (2009) 165–174.
[4] T. Guillon, J. Schaefer, Rotational-echo double-resonance NMR, J. Magn. Reson. 81 (1988) 196–200.
[5] B.H. Meier, W.L. Earl, Excitation of multiple quantum transitions under magic-angle conditions: adamantine, J. Chem. Phys. 85 (1986) 4905–4911.
[6] T.G. Oas, R.G. Griffin, M.H. Levitt, Rotary resonance recoupling of dipolar interactions in solid-state nuclear magnetic resonance spectroscopy, J. Chem. Phys. 89 (1988) 692–695.
[7] R. Tycko, G. Dabbagh, Measurement of nuclear magnetic dipole–dipole couplings in magic-angle spinning NMR, Chem. Phys. Lett. 173 (1990) 461–465.
[8] W. Sommer, J. Gottwald, D.E. Demco, H.W. Spiess, Dipolar heteronuclear multiple-quantum NMR spectroscopy in rotating solids, J. Magn. Reson. A 113 (1995) 131–134.
[9] M. Feike, D.E. Demco, R. Graf, J. Gottwald, S. Hafner, H.W. Spiess, Broadband multiple-quantum NMR spectroscopy, J. Magn. Reson. A 122 (1996) 214–221.
[10] N.C. Nielsen, H. Bildsoe, H.J. Jakobsen, M.H. Levitt, Double-quantum homonuclear rotary resonance: efficient dipolar recovery in magic angle spinning, J. Chem. Phys. 101 (1994) 1805–1812.
[11] Y.K. Lee, N.D. Kurur, M. Helmle, O.G. Johannessen, N.C. Nielsen, M.H. Levitt, Efficient dipolar recoupling in the NMR of rotating solids: a seven-fold symmetric radiofrequency pulse sequence, Chem. Phys. Lett. 242 (1995) 304–309.
[12] M. Carravetta, M. Edén, X. Zhao, A. Brinkmann, M.H. Levitt, Symmetry principles for the design of radiofrequency pulse sequences in the nuclear magnetic resonance of rotating solids, Chem. Phys. Lett. 321 (2000) 205–215.
[13] A. Brinkmann, M. Edén, M.H. Levitt, Synchronous helical pulse sequences in magic-angle spinning nuclear magnetic resonance: double quantum recoupling of multiple-spin systems, J. Chem. Phys. 112 (2000) 8539–8554.
[14] Y. Ishii, $^{13}C–^{13}C$ dipolar recoupling under very fast magic angle spinning in solid state nuclear magnetic resonance: applications to distance measurements, spectral assignments and high-throughput secondary-structure determination, J. Chem. Phys. 114 (19) (2001) 8473–8483.
[15] M.H. Levitt, Symmetry-based pulse sequences in magic-angle spinning NMR, in: D.M. Grant, R.K. Harris (Eds.), Encyclopedia of nuclear magnetic resonance, vol. 9, John Wiley & sons, Chichester, 2002.
[16] P.E. Kristiansen, M. Carravetta, J.D. van Beek, W.C. Lai, M.H. Levitt, Theory and applications of super-cycled symmetry-based recoupling sequences in solid-state NMR, J. Chem. Phys. 12 (2006) 234510–234519.
[17] G. Pileio, M. Concistrè, N. McLean, A. Gansmüller, R.C.D. Brown, M.H. Levitt, Analytical theory of γ-encoded double-quantum recoupling sequences in solid-state nuclear magnetic resonance, J. Magn. Reson. 186 (2007) 65–74.
[18] L. Mafra, R. Siegel, C. Fernandez, D. Schneider, F. Aussenac, J. Rocha, High-resolution ^1H homonuclear dipolar recoupling NMR spectra of biological solids at MAS rates up to 67 kHz, J. Magn. Reson. 199 (2009) 111–114.
[19] B. Hu, Q. Wang, O. Lafon, J. Trébosc, F. Deng, J.P. Amoureux, Robust and efficient spin-locked symmetry-based double-quantum homonuclear dipolar recoupling for probing $^1H–^1H$ proximity in the solid state, J. Magn. Reson. 198 (2009) 41–48.
[20] B. Hu, L. Delevoye, O. Lafon, J. Trébosc, J.P. Amoureux, Double-quantum NMR spectroscopy of ^{31}P species submitted to very large CSAs, J. Magn. Reson. 200 (2009) 178–188.
[21] Q. Wang, B. Hu, O. Lafon, J. Trébosc, F. Deng, J.P. Amoureux, Double-quantum homonuclear NMR correlation spectroscopy of quadrupolar nuclei subjected to magic-angle spinning and high magnetic field, J. Magn. Reson. 200 (2009) 251–260.
[22] Q. Wang, B. Hu, F. Fayon, J. Trébosc, C. Legein, O. Lafon, F. Deng, J.P. Amoureux, Double-quantum $^{19}F–^{19}F$ dipolar recoupling at ultra-fast magic angle spinning NMR: application to the assignment of ^{19}F NMR spectra of inorganic fluorides, Phys. Chem. Chem. Phys. 11 (2009) 10391–10395.
[23] I. Schnell, Dipolar recoupling in fast MAS solid-state NMR spectroscopy, Prog. Nucl. Magn. Reson. Spectrosc. 45 (2004) 145–207.
[24] S.P. Brown, Probing proton–proton proximities in the solid state, Prog. Nucl. Magn. Reson. Spectrosc. 50 (2007) 199–251.
[25] C.D. Martin, S. Chaudhuri, C.P. Grey, J.B. Parise, Effect of A-site cation radius on ordering of BX6 octahedra in (K, Na)MgF3 perovskite, Am. Mineral. 90 (2005) 1522–1533.
[26] C. Martineau, C. Legein, J.Y. Buzaré, F. Fayon, On the assignment of ^{19}F MAS NMR spectra of fluoroaluminates using through-space spectral edition of $^{19}F–^{27}Al$ and $^{19}F–^{19}F$ connectivities, Phys. Chem. Chem. Phys. 11 (2009) 950–957.
[27] A. Brinkmann, M.H. Levitt, Symmetry principles in the nuclear magnetic resonance of spinning solids: hetero-nuclear recoupling by generalized Hartmann–Hahn sequences, J. Chem. Phys. 115 (2001) 357–384.
[28] M. Edén, M.H. Levitt, Pulse sequence symmetries in the NMR of spinning solids. Application to heteronuclear decoupling, J. Chem. Phys. 111 (1999) 1511–1519.
[29] [a] Wolfram Research Inc., Champaign, Illinois, USA, 2007. Mathematica 6. Available from: <http://reference.wolfram.com/mathematica/ref>.;
[b] 'C and R symmetries' Mathematica package written by M.H. Levitt and A. Brinkmann. Available from: <http://www.mhl.soton.ac.uk/public/Main/software/CandRsymmetries/index.html> and <http://www.mhl.soton.ac.uk/public/Main/software/mPackages/UpdateInformation.html>.
[30] M. Edén, D. Zhou, J. Yu, Improved double-quantum NMR correlation spectroscopy of dipolar-coupled quadrupolar spins, Chem. Phys. Lett. 431 (2006) 397–403.
[31] M. Carravetta, M. Eden, O.G. Johannessen, H. Luthman, P.J.E. Verdegem, J. Lugtenburg, A. Sebald, M.H. Levitt, Estimation of carbon–carbon bond lengths and medium-range inter-nuclear distances by solid-state nuclear magnetic resonance, J. Am. Chem. Soc. 123 (2001) 10628–10638.
[32] (a) M.H. Levitt, Composite pulses, Prog. NMR Spectrosc. 18 (1986);
(b) M.H. Levitt, Composite pulses, in: D.M. Grant, R.K. Harris (Eds.), Encyclopedia of Nuclear Magnetic Resonance, John Wiley & sons, Chichester, 2002, pp. 1396–1410.
[33] A. Brinkmann, M. Eden, Second order average Hamiltonian theory of symmetry-based pulse schemes in the nuclear magnetic resonance of rotating solids: application to triple-quantum dipolar recoupling, J. Chem. Phys. 120 (2004) 11726.
[34] T. Karlsson, A. Brinkmann, P.J.E. Verdegem, J. Lugtenburg, M.H. Levitt, Multiple-quantum relaxation in the magic-angle-spinning NMR of ^{13}C spin pairs, Solid State Nucl. Magn. Reson. 14 (1999) 43–58.
[35] G. Mali, G. Fink, F. Taulelle, Double-quantum homonuclear correlation magic-angle sample spinning nuclear magnetic resonance spectroscopy of dipolar-coupled quadrupolar nuclei, J. Chem. Phys. 120 (2004) 2835–2845.
[36] K. Riedel, C. Herbst, J. Leppert, O. Ohlenschläger, M. Görlach, R. Ramachandran, Broadband homonuclear double-quantum NMR/filtering via zero-quantum dipolar recoupling in rotating solids, Chem. Phys. Lett. 424 (2006) 178–183.
[37] M. Bak, J.T. Rasmussen, N.C. Nielsen, SIMPSON: a general simulation program for solid-state NMR spectroscopy, J. Magn. Reson. 147 (2000) 296–330.
[38] M. Bak, N.C. Nielsen, REPULSION: a novel approach to efficient powder averaging in solid-state NMR, J. Magn. Reson. 125 (1997) 132–139.
[39] A. Zheng, S.B. Liu, F. Deng, ^{19}F chemical shift of crystalline metal fluorides: theoretical predictions based on periodic structure models, J. Phys. Chem. C 113 (33) (2009) 15018–15023.
[40] A. Hémon, G. Courbion, Refinement of the room temperature structure of α-$CaAlF_5$, Acta. Crystallogr. C47 (1991) 1302–1303.
[41] A. Le Bail, G. Férey, A.M. Mercier, A. de Kozak, M. Samouël, Structure determination of β and γ-$BaAlF_5$ by X-ray and neutron powder diffraction. A model for the α → β → γ transitions, J. Solid State Chem. 89 (1990) 282–291.
[42] V. Kaiser, D. Babel, Crystal structure of $Ba_3Al_2F_{12}$, Z. Anorg. Allg. Chem. 630 (2004) 794–798.
[43] D. States, R. Haberkorn, D. Rubens, A two-dimensional Nuclear Overhauser Experiment with pure absorption phase in four quadrants, J. Magn. Reson. 48 (1982) 286–292.
[44] M. Leskes, P.K. Madhu, S. Vega, Super-cycled homo-nuclear dipolar decoupling in solid state NMR: toward cleaner ^1H spectrum and higher spinning rates, J. Chem. Phys. 128 (2008) 052309.
[45] E. Salager, R.S. Stein, S. Steuernagel, A. Lesage, B. Elena, L. Emsley, Enhanced sensitivity in high-resolution ^1H solid-state NMR spectroscopy with DUMBO dipolar decoupling under ultra-fast MAS, Chem. Phys. Lett. 469 (2009) 336–341.

[46] J.P. Amoureux, B. Hu, J. Trebosc, Enhanced resolution in proton solid-state NMR with very-fast MAS experiments, J. Magn. Reson. 193 (2008) 305–307.
[47] M.J. Bayro, M. Huber, R. Ramachandran, T.C. Davenport, B.H. Meier, M. Ernst, R.G. Griffin, Dipolar truncation in magic-angle spinning NMR recoupling experiments, J. Chem. Phys. 130 (2009) 114506.
[48] V. Ladizhansky, Homonuclear dipolar recoupling techniques for structure determination in uniformly ^{13}C-labeled proteins, Solid State NMR 36 (2009) 119–128.
[49] (a) N. Khaneja, N.C. Nielsen, Triple oscillating field technique for accurate distance measurements by solid-state NMR, J. Chem. Phys. 128 (2008) 015103; (b) L.A. Straasø, M. Bjerring, N. Khaneja, N.C. Nielsen, Multiple-oscillating-field techniques for accurate distance measurements by solid-state NMR, J. Chem. Phys. 130 (2009) 225103.
[50] A.K. Paravastu, R. Tycko, Frequency-selective homonuclear dipolar recoupling in solid state NMR, J. Chem. Phys. 124 (2006) 194303.